Deep–Sea Research I 224 (2025) 104557

Contents lists available at ScienceDirect

Deep-Sea Research Part I

journal homepage: www.elsevier.com/locate/dsri

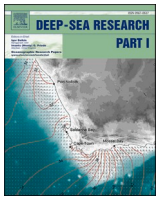

Evaluating the role of physical mechanisms as possible triggers for turbidity currents in a deep ocean seamount

Susana M. Lebreiro [a,*], Álvaro Peliz [b], Laura Antón [c], Sílvia Nave [d], M. Isabel Reguera [a], Rocío Lozano-Luz [a], Claire Waelbroeck [e], Simon Crowhurst [f], Belen Martrat [g], Jordi F. Lopez [g], Raphaël Hebert [h], Alejandra Lopez-Rodriguez [a]

[a] Instituto Geológico y Minero de España (IGME CN) CSIC, Research Group of Sedimentary Record of Paleoclimate Changes, Dept. GeoHazards and Climate Change, Calle Ríos Rosas, 23, 28003, Madrid, Spain
[b] Instituto Dom Luiz, Faculdade de Ciências da Universidade de Lisboa, Campo Grande, 1749-016, Lisboa, Portugal
[c] Instituto Geológico y Minero de España (IGME CN) CSIC, Research Group of Sedimentary Record of Paleoclimate Changes, Dept. GeoHazards and Climate Change, Calle Calera, 1, Tres Cantos, Madrid, 28760, Spain
[d] Laboratório Nacional de Energia e Geologia (LNEG). Geology, Hydrogeology and Coastal Geology Unit. Estrada da Portela, Bairro do Zambujal Ap.7586. 2610-999, Amadora, Portugal
[e] LOCEAN - IPSL (UMR 7159 CNRS/IRD/SU/MNHN), 4 Place Jussieu, BP 100, 75252 Paris Cedex 05, France
[f] The Godwin Laboratory for Paleoclimate Research, University of Cambridge, Dept. of Earth Sciences, Downing Street, CB2 3EQ, Cambridge, United Kingdom
[g] Instituto de Diagnóstico Ambiental y Estudios del Agua (IDAEA) CSIC, Dept. of Environmental Chemistry, Calle Jordi Girona 18-26, 08034, Barcelona, Spain
[h] Alfred Wegener Institute, Helmholtz Centre for Polar and Marine Research, Telegrafenberg A45, 14473, Potsdam, Germany

A B S T R A C T

Turbidity currents on continental margins are often attributed to cyclic climate variability and sea-level change, while the causes of deep ocean turbidites are as yet to be tested. The Atlantic Iberian margin provides a unique setting to contrast deep ocean and continental environments, including depression features that further protect from resuspension and erosion by along-slope bottom currents. We present records of low-frequency, non-periodic, climate-independent turbidites from three deep cores covering up to 426,000 years in the Tore seamounts area. By evaluating a range of physical oceanographic mechanisms, the breaking of internal waves and mesoscale Mediterranean-eddies against unstable slopes in the seamounts area arises as the most likely triggers that precondition the recurrence pattern of the observed deep ocean turbidites.

1. Introduction

The deep sea experiences the occasional, geologically instantaneous emplacement of turbidite deposits originating from unstable seabed slopes (e.g., Gamboa et al., 2021). Sediment transport by turbidity currents is an important process that threatens critical global infrastructure such as submarine telecommunication cables, pipelines, or platforms in shallow and deep waters (e.g., Carter et al., 2014). Seldom discussed and of interest in this study are the triggering mechanisms for turbidity currents decoupled from continental margin sedimentary processes.

The recurrence and frequency of turbidites in the geological record emanating from the passive Portuguese continental margin have usually been attributed to major triggers such as eustatic sea-level shifts forced by climatic changes on different time scales (e.g., Lebreiro et al., 1997, 2009), in parallel with devastating episodes of seismic shaking (e.g., Gràcia et al., 2010; Masson et al., 2011).

The former corresponds to the model of continental shelf exposure to erosion during low sea-level stands when submarine canyons develop, and turbidity currents and landslides transfer sediments to the deep ocean after accumulation during high sea-level stands (Vail et al., 1979; Shanmugam and Moiola, 1982; Posamentier and Vail, 1988; Nisbet and Piper, 1998; Owen et al., 2007; Knudson and Hendy, 2009). However, near the influence of continental margins, not only eustatic low-stands, but also the rising and falling of sea-level have been invoked to explain the occurrence of turbidites. On the Atlantic Iberian and Celtic-Armorican margins, millennial climate variability of Heinrich (Bond et al., 1993; Rahmstorf, 2003) and Dansgaard-Oeschger

* Corresponding author.
E-mail addresses: susana.lebreiro@igme.es (S.M. Lebreiro), ajpeliz@fc.ul.pt (Á. Peliz), l.anton@igme.es (L. Antón), silvia.nave@lneg.pt (S. Nave), mi.reguera@igme.es (M.I. Reguera), rociolozanoluz@gmail.com (R. Lozano-Luz), claire.waelbroeck@locean.ipsl.fr (C. Waelbroeck), sjc13@cam.ac.uk (S. Crowhurst), belen.martrat@idaea.csic.es (B. Martrat), jordi.lopez@idaea.csic.es (J.F. Lopez), raphael.hebert@awi.de (R. Hebert), mariaalejandra.lopez@igme.es (A. Lopez-Rodriguez).

https://doi.org/10.1016/j.dsr.2025.104557
Received 21 December 2024; Received in revised form 15 June 2025; Accepted 16 July 2025
Available online 19 July 2025

(Dansgaard et al., 1993; Grootes et al., 1993) extreme cold events, related to minor sea-level changes (Siddall et al., 2008), have also shown significant impact on higher frequencies of turbidites (Toucanne et al., 2008; Lebreiro et al., 2009). Farther from the continental margins, for instance on the Atlantic Madeira Abyssal Plain (Weaver and Kuijpers, 1983; Weaver et al., 1992), if only white-carbonate turbidites originating from the nearby Mid-Atlantic Ridge and surrounding seamounts are considered, which thus exclude continental margin supply triggers, the recurrence would account 1 turbidite every 150 ka for the last 750 ka. While it is true that some of these turbidites coincide either with glaciations and deglaciations during the early Pleistocene (Weaver and Kuijpers, 1983; Weaver et al., 1992) or with rising sea-levels and high-stands in a long 17 Ma-series of volcaniclastic turbidites originating from the flank collapse of the Canary Islands (Hunt et al., 2014), an increasing body of evidence suggests that there is no statistically significant association between these events and changes in sea-level and related climate (Urlaub et al., 2013; Hunt et al., 2014). In addition, from a geomechanical perspective, the potential effect of slow sea-level fluctuations on slope stability and failure is reduced, as the hydrostatic pore water pressure and total stress on the seafloor are minimised with increasing water depth (Urlaub et al., 2013). This poses the challenge of explaining non-periodic, low-frequency deep sea turbidite series on a regional scale, addressing a knowledge gap that the present study aims to fill.

Seismic shaking is considered to be the second major trigger of turbidity currents, sustained by the regional spatial distribution of synchronous turbidite deposits. Paleoseismites have been reported in the Portuguese margin, ultimately related to the well-known 1755 Lisbon earthquake and other instrumental and historical seismic events, but always associated with submarine canyon systems attached to the continental margin (Lebreiro et al., 1997; Gràcia et al., 2010; Masson et al., 2011). Assigning seismicity as a primary external trigger for turbidity currents is not unequivocal (Masson et al., 2011) and requires careful tracing of their source areas and validation of the regional correlation of individual simultaneous turbidites (e.g., Goldfinger et al., 2007; Gràcia et al., 2010; Mérindol et al., 2022).

On the other hand, major external triggers such as sea-level changes, earthquakes and other triggers (seasonal storms, surface and internal tides, or intensive fishing) have been rejected as explanations for more than 1000 land-detached Whittard-type submarine canyon systems monitored over a period of time (Heijnen et al., 2022), which are certainly more influenced by continental sedimentary processes than the far-land and abyssal setting of our cores. Finding non-correlatable and inconsistent records, Heijnen et al. (2022) relegated the possibility of the occurrence of turbidity currents to a sustained or sudden preconditioned sediment supply, where a number of minor perturbations are sufficient to initiate a turbidity current. This is, in turn, contradictory to the direct irrelevance of rapid sedimentation rates in preconditioning slope failure, as argued by Urlaub et al. (2013). Besides, for the nearby Nazaré Canyon, Allin et al. (2016) discerned the discrepancy in the frequency of canyon-filling (triggered by sea–level change, storms and nepheloid transport) and canyon-flushing events. In their study, a random process or signal shredding (i.e., attenuation of the environmental signal by non-linear sediment transport processes; Jerolmack and Paola, 2010) is further introduced as a solution to explain this difference (Allin et al., 2016).

Recognising the above ambiguities and controversies, which may be partly strengthened by uncertainties in statistical analysis (Allin et al., 2017), we focus on the need for alternative mechanisms capable of triggering turbidity currents in the deep ocean other than those commonly attributed to continental margins.

We examine several physical oceanographic processes that would affect the deep domain of the Tore seamounts area from global and regional perspectives, in particular the influence of internal tides, or internal waves, over complex topography. The capacity of internal waves to trigger turbidity currents has already been demonstrated in submarine valleys and canyons (Miramontes et al., 2019; Heijnen et al., 2022), as has the converse (Azpiroz-Zabala et al., 2017), thereby illustrating their potential.

The seabed is covered with seamounts affected by oscillations varying from lower to higher frequencies in a large spectrum of periodicities: inertial oscillations (a function of latitude), diurnal- and semi-diurnal- tides (23.93 h, K_1; and 12.42 h, M_2 tidal components, respectively), and buoyancy-forced motions (a function of local ocean stratification) (Lavelle and Mohn, 2010). Internal tides (i.e. internal waves of tidal frequencies) are generated by the interaction of barotropic tides with topography in a stratified ocean. Rougher topography and greater stratification increase internal wave activity and mixing (Polzin et al., 1997). In the deep sea, seamounts act as sources and sinks of eddies and are the main features converting periodic processes (ocean tides) into higher-frequency waves and ultimately turbulence (Lavelle and Mohn, 2010). Despite the substantial number of seamounts distributed across abyssal settings (e.g., isolated basins such as Tore), their role as turbidite sources remains under-explored, and their triggers remain speculative.

Several processes operate on abyssal circulation, including the transfer of energy from mesoscale to small-scale processes including diapycnal mixing in the deep ocean (Liang and Thurnherr, 2012), mean flow–seamount interaction over crests and slopes (Ledwell et al., 2000; Lavelle and Mohn, 2010), internal wave shear-induced mixing (MacKinnon et al., 2017), mesoscale eddy–seamount collisions (Bell, 1975; Richardson et al., 2000), and occasional internal wave breaking near steep slopes (Polzin, 2009; van Haren, 2018). However, these have only been marginally linked to sediment erosion/deposition in the deep ocean, notwithstanding work from Lonsdale et al. (1976) to Turnewitsch et al. (2013) and van Haren et al. (2015).

We provide three new time series of turbidites from tactical deep ocean environments in the Atlantic Iberian margin to test whether internal ocean processes precondition slope failure and turbidity triggering in the deep sea. By combining sediment core records, numerical model simulations of tidally driven circulation over deep sea topography and realistic mesoscale flow, and CTD observations, we introduce methodological innovations that help to resolve debates on abyssal sediment dynamics.

2. Materials and methods

2.1. Core sites

Calypso core MD13-3473 (39°22.680′ N; 12°50.114′ W) was collected at −5505 m in the basin surrounded by the Tore seamounts, in the absence of resuspension and erosion by along-slope bottom currents (Fig. 1a, Table S1). This internal basin, with a depth of −5505 m and a diameter of 120 × 90 km, has summits at −2200 m below the sea surface and is externally isolated except for two narrow sills that reach depths of −4300 m. Morphologically, it emerges from the surrounding abyssal floor and is 300 km from the Portuguese continental margin, providing an opportunity to analyse a record set aside of continental margin-associated sedimentary processes. Giant piston core D219/3P (39°18.03′N; 11°21.31′W) was collected at −4860 m in the Rincão da Pomba basin, positioned between the Iberian margin and the Tore seamount (Fig. 1a), and collects sediments from the surrounding seamounts and, eventually, continental slopes. Piston core D11956 T/P (38°21.9′N; 12°35.6′W) was recovered at −4825 m in the distal Tagus Abyssal Plain, adjacent to the SE outer flank of the Tore seamounts. It is reached by turbidity currents that may originate both at the summit rim and outer slopes of the Tore seamounts and at the continental margin via the Tagus and Sado submarine canyons after a run-out distance of 300 km (Lebreiro, 1995). No sediment transport pathways connect these three sites. Calypso core MD03-2698 (38°14.37′N; 10°23.42′W), taken from the Iberian margin at a water depth of −4602 m, is used here as a contrasting continental reference core (Lebreiro et al., 2009).

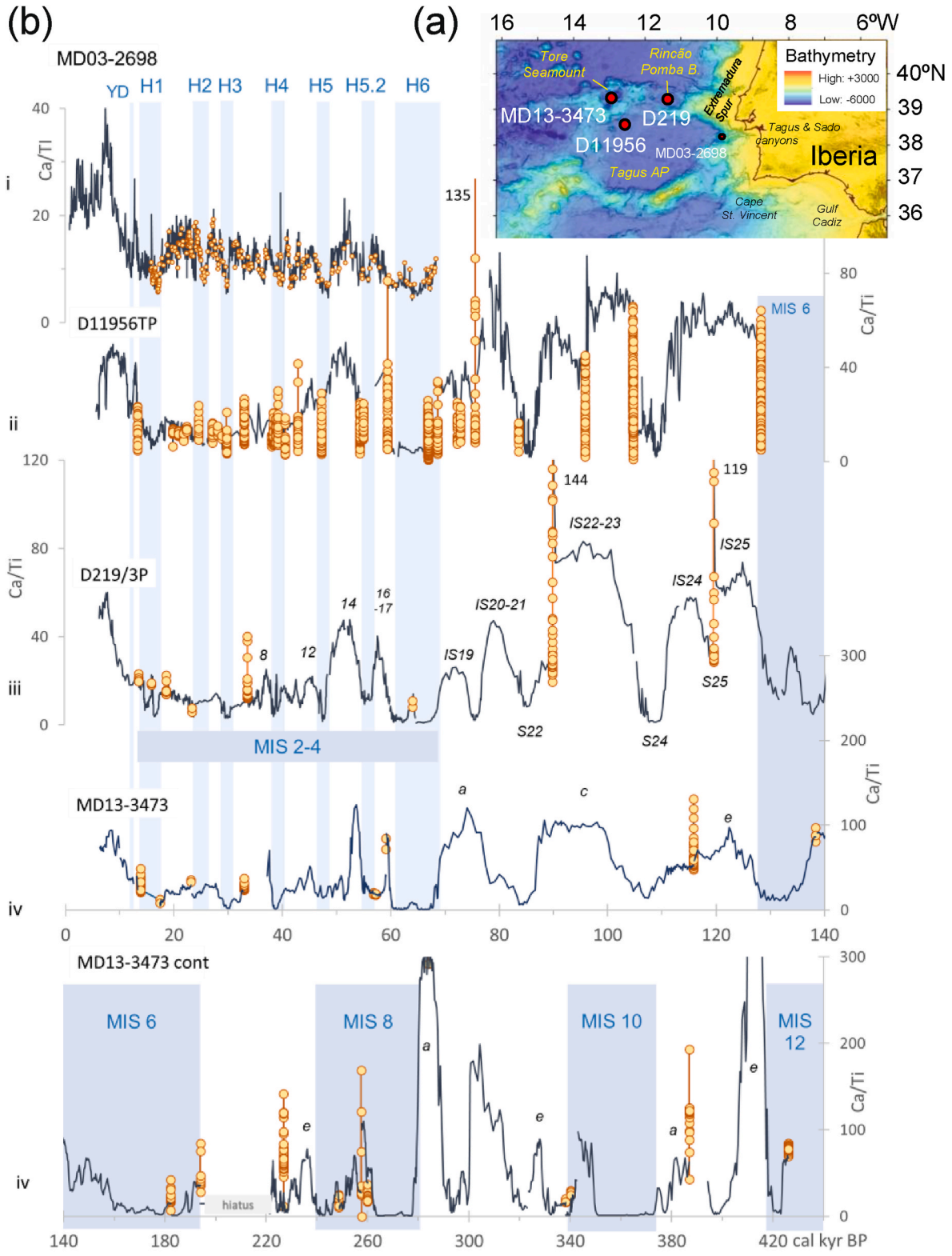

Fig. 1. Turbidite series setting from −5000 m in the deep ocean off the Iberian margin over the past 426 ky. (a) Location of marine cores MD13-3473, D219/3P, and D11956 T/P; reference core MD03-2698 is also shown. Bathymetry in metres, from GEBCO. (b) Contrast between non-periodic sedimentary records of turbidites deposited off the Iberian margin and a cyclic record from the continental margin. From top to bottom: (i) MD03-2698, which is an example of a millennial-scale climate-dependent turbidite series from the continental margin (see Suppl. Material); (ii) D11956 T/P from the distal Tagus Abyssal Plain on the outer SE flank of the Tore seamounts; (iii) D219/3P from the Rincão da Pomba basin located between the Tore seamounts and the continental margin, and (iv) MD13-3473 from the internal basin of the Tore seamounts. Ca/Ti oscillations (blue line, X-ray fluorescence at 1 cm resolution) depict carbonate sedimentation during interglacial and glacial stages (darker blue rectangles for glacials, and light blue bars for the Younger Dryas (YD) and Heinrich (H) cold events (Bond et al., 1993; Rahmstorf, 2003)). The orange circles symbolise turbidites, and the length of the lines is proportional to the thickness of each turbidite. Note that turbidites are represented by vertical lines as they respond to geologically instant deposition. MIS stands for Marine Isotope Stage and a-c-e represent warm substages. (For interpretation of the references to colour in this figure legend, the reader is referred to the Web version of this article.)

2.2. Ca/Ti curves

The split halves of the cores were carefully scraped and covered with 40 micron-thick "Ultralene" film and flattened to the sediment surface to remove any air bubbles trapped underneath. These sections were then analysed by using non-destructive, continuous X-ray fluorescence (XRF), with an irradiated area of 5 mm in length (down-core) and 12 mm in width (cross-core). The full length of MD13-3473 was measured every 1 cm using an Avaatech core scanner at the University of Barcelona, Spain. Spectra were processed using WinAxiBatch software. The SMAR4 standard supplied by Avaatech (Analytical X-ray Technology, The Netherlands) was used for external calibration. Two replicates were performed along each of the sixteen 1.5 m long sections.

For cores D219/3P and D11956 T/P, the resolution was 1 cm and 2 mm respectively, and were measured at BOSCORF, National Oceanography Center, UK, using a COX Analytical Systems Itrax X-ray Fluorescence (XRF) scanner, while the data were processed using the supplied bAxil software.

The elements considered here (Ca, Ti, Zr, Sr, and Rb) were extracted from a series of 15 (10 kV), 17 (30 kV) and 7 (50 kV) elements (Lebreiro et al., 2025d,e,f,g,h).

2.3. Stratigraphy, timing of turbidites and estimation of frequency

Turbidites are the result of geologically instantaneous events. Their facies exhibit homogeneous chemical characteristics, as determined by colour change and XRF-elemental ratios, and show bioturbation at the top and sharp erosive sandy-silt bases at the bottom. As the term 'tidalites' is vaguely defined and their facies are mostly indistinguishable (Shanmugam, 2021), we prefer to refer to the facies presented in this study as turbidites. To develop the time frame for the turbidite units, facies were identified together with the hemipelagic sedimentary record. Turbidites can be extracted (stratigraphically removed) from the hemipelagic curve without compromising the quality of the sections used for stratigraphy and paleoceanography. The hemipelagic stratigraphy was constructed using XRF Ca/Ti, Zr/Sr (biogenic and detrital proxies; Dypvik and Harris, 2001; Wu et al., 2020) and $\delta^{18}O$ of benthic foraminifera (ice volume and temperature proxy) (Fig. S1; Lebreiro et al., 2025k). The result of our methodological procedure is a well-timed long series of turbidite deposition for the three deep ocean cores.

The age models and sedimentation rates of cores MD13-3473, D219/3P, and D11956 T/P (Suppl. Material, Figs. S1–S6; Lebreiro et al., 2025a,b,c,j), were constrained for the hemipelagic sediment by interpolation between fixed depths dated by AMS ^{14}C (Table S2) together with age-depth pointers aligned with high-resolution chronostratigraphic reference sequences in the area, such as MD03-2698 (Lebreiro et al., 2009, 2025f; Waelbroeck et al., 2019, 2023; 2022: SEANOE database: doi.org/10.17882/59554), SHAK05-3P, U1385 and MD01-2444/2443 (Hodell et al., 2015), and MD01-2446 (Voelker et al., 2010; Nave et al., 2019) (Fig. S1; Table S3). Sedimentation rates are assumed to be constant between fixed dated depths. To date the turbidites, the interpolated age corresponding to the 1 cm layer above the top of each turbidite is assigned as the age of the turbidite after the turbidite units were restored to the hemipelagic stratigraphy (Table S4). We considered the erosion caused by occasional turbidite deposition to be negligible, as reported for the Iberian surrounding abyssal plains (Weaver and Kuijpers, 1983; Lebreiro et al., 1997; Vizcaíno et al., 2006) and the margins of North America (Goldfinger et al., 2007; Gutierrez-Pastor et al., 2009; Mérindol et al., 2022). The average frequency of turbidites is estimated by the number of events per core length in thousands of years (Table 1). The depth and thickness of each turbidite are given in Table S4. The datasets are stored in the PANGAEA-Publisher for Earth & Environmental Science repository (Felden et al., 2023).

Table 1
Number of turbidites per core, thickness, and average frequency.

	MD13-3473	D219/3P	D11956 T/P	MD03-2698
# turb/core	19	8	41	262
Minimum thickness of turbidite (m)	0.01	0.01	0.01	0.001
Maximum thickness of turbidite (m)	2.003	2.72	0.37	0.04
Thickness average of turbidite (m)	0.41	0.49	0.13	0.002
Frequency (turbidite/ky[a])	1/22	1/18	1/3	1/0.258
Length of core (m)	23.90	15.43	8.44 (piston) +0.34 (trigger)	35.40

[a] ky for thousands of years.

2.4. CTD

CTD data were collected in the Tore basin during cruises ARCANE-Action Recherche Circulation Atlantique in 1998 (Le Cann et al., 2000) and Eurofleets-TORE in 2013 (Nave et al., 2013). In the latter, the SEABIRD SBE 911Plus System equipped with a 24-bottle carousel water sampler (SBE32) was deployed for the upper −3000 m, while a CTD coupled to the head of the Casq corer was used for the −5000 m depth (Nave et al., 2013). CTD profiles are available from the IFREMER oceanographic data repository.

2.5. Numerical model studies

Simulations were produced with the Regional Ocean Modelling System (ROMS) (Shchepetkin and McWilliams, 2005a,b) to investigate the flow–topography interactions around the Tore seamounts, considering tidal forcing only and mesoscale flows. In the case of tidal forcing, simulations are initialised with a laterally homogeneous climatological density stratification. The model was forced with tidal constituents from TPXO (https://www.tpxo.net/global) (global tidal model amplitudes and phases: M_2, S_2, N_2, K_2, K_1 and O_1). No surface fluxes were imposed. The domain limits may be sensitive to remotely generated baroclinic tidal energy. The option to include the shelf in the domain was motivated by the identification of internal tide generation over the promontory. Additionally, the shelf to the east helped to reduce the strong velocities along the eastern boundary associated with Kelvin wave propagation. The meridional and zonal dimensions of the domain were selected to allow the internal tide to propagate away from the Tore seamounts (Fig. S7). The southern, western, and northern boundaries were open, and a set of radiative (Orlansky) conditions for 3D momentum and tracers, Flather for 2D variables and passive/active nudging type conditions were used. The solutions along the boundaries were also complemented with a sponge layer for viscosity and diffusivity. The horizontal resolution was 1/90° (<1 km), and the 100 sigma layers had stretching factors $\theta_b = 0$ and hc = 20. A linear bottom drag parameterization was used (Cd = $3x10^{-4}$ m/s). The diffusion and viscosity in the sponge area were applied using Laplacian operators along geopotential surfaces. Surface and bottom boundary layers (BBL) were parameterized using KPP. Tidal simulations are two-months long, and the results presented are the averages over the entire simulation period.

The second simulation used in this study is a high-resolution (~1 km) regional circulation model aimed at studying mesoscale flow patterns associated with Mediterranean water in the Atlantic. Representing the Mediterranean undercurrent requires a higher vertical resolution, so a greater number of sigma layers (80) is used. The model does not include tides, and the simulations span a period of six months following a three-year spin-up. These simulations build on two decades of accumulated experience in regional circulation simulations of the Mediterranean outflow (e.g., Peliz et al., 2007; Peliz et al., 2013). These are rather complex simulations, so for the sake of brevity, we refer interested

readers to these studies for a detailed description of the model. The updates relative to previous modelling versions are essentially related to higher resolutions and numerical implementations aligned with the current standard of CROCO version V1.2.

However, it is worth noting that, in relation to this study, sigma-coordinate models such as ROMS always produce spurious flow over steep topography (not necessarily over the bottom itself), particularly in those parts of the water column where steep model layers coincide with high buoyancy gradients. These errors can be minimised either by using less vertical resolution (a lower number of sigma-layers) or smoother topographies.

These errors manifest as rim-like or contour (along-isobath) time-mean currents, which, in extreme cases, can reach a few centimetres per second.

In the case of Tore, we aimed for values below 1 cm/s, and we will discuss the possible impact on the validity of the results below.

3. Results and discussion

3.1. Deep ocean turbidite records

The mid-latitude Iberian margin has yielded key turbidite datasets interbedded with Late Quaternary hemipelagites at unusual water depths of approximately −5000 m, and precluding the potential influence of land-attached canyon systems. The sediment cores studied come from three exclusive deep basins: MD13-3473 (Tore seamounts semi-enclosed basin), D219/3P (Rincão da Pomba basin) and D11956 T/P (distal Tagus Abyssal Plain) (Fig. 1a; Table S1). The previously published dataset MD03-2698 on the levee of the Tagus and Sado river canyon system, which is thus connected to land (Lebreiro et al., 2009), is used here as a comparison site, where clusters of increasing turbidites responding to millennial-scale cyclicity clearly dissent from the new sites.

Sources and frequency of turbidites - The turbidites found at MD13-3473 (Tore basin) can only be triggered from the rim and inner slopes of the Tore seamounts deeper than −2200 m, where the potential effect of sea-level fluctuations on slope stability and failure is somewhat reduced (Urlaub et al., 2013). Together with a discontinuous pattern and a slow average frequency of 1 turbidite/22 ky (Table 1), this semi-enclosed site ensures entire independence from continental sedimentary processes and sea-level climate change related forcing.

The other two series, although most likely influenced by mixed continental and deep ocean processes, also show discontinuous deposition of turbidites. Core D219/3P (Rincão da Pomba basin) collects turbidites from the slopes of nearby seamounts and has an average frequency of 1 turbidite/18 ky. Further away, D11956 T/P (Tagus Abyssal Plain) is reached by turbidity currents that have initiated on the summit rim and outer slopes of the Tore seamounts, as well as on the continental margin via the Tagus and Sado submarine canyons (Lebreiro, 1995), with an average frequency of 1 turbidite/3 ky.

Our results show no linear relationship between the turbidite deposition and continental shelf proximity as deduced from the lowest and highest frequencies of nearby MD13-3473 and D11956 T/P, respectively. The few analogies between site D11956 T/P (partly fed by canyons) and MD03-2698 (at the levee and fully supplied by a canyon) suggest that submarine canyons may play a role in partially explaining the relatively higher frequency of turbidites sourced in the continent (Lebreiro et al., 2009) (Fig. 1b).

Timing of turbidites – The three new series of turbidites are detailed in the Supplementary Material (Table S3; Table S4). The MD13-3473 sequence spans 426 ky with nineteen individual turbidites up to 2 m thick, covering five orbital glacial-interglacial cycles (Fig. 1b–iv). There is no coherence between the emplaced turbidites and either (sub)orbital (full glacial low sea-level stand *versus* full interglacial high sea-level stand, including warmer/cooler substages) or millennial time scales (Fig. 1b–iv). D219/3P covers 141 ky and contains eight turbidites of variable thickness exceeding 2.7 m (Fig. 1b–iii). D11956T/P extends back to MIS-5 through 128 ky, with a record of forty-one turbidites and an average thickness (maximum thickness of 0.37 m; Table 1) that is the lowest of the three series (Fig. 1b–ii).

These findings contrast with those of continental margin studies, particularly core MD03-2698, which 2- to 4-fold higher sedimentation rate during the last glacial low-stand compared to the Holocene high-stand, exhibited a turbidite record that is climate-dependent, with a coherent pattern of increasing frequency of very thin turbidites (average frequency of 1 every 258 years; Table 1; Lebreiro et al., 2025i) concentrated in clusters preferentially during Heinrich stadials H6 to 1 and Greenland stadial events over the last 63 ky (Lebreiro et al., 2009) (Fig. 1b–I; Fig. S3). These are also linked to sea-level oscillations and rapid shifts in global circulation in the Atlantic (Lebreiro et al., 2009).

Regardless of the distance between our land-detached sites, the frequency and timing of turbidites reveal non-periodic series in all three records. There is no consistent, predictable pattern in these three new series, with only a few temporal coincidences occurring during millennial-scale climate events or suborbital transitions. Given the absence of turbidites during H3, H4 and H5 in both MD13-3473 and D219/3P, and over older sections of the last five glacial–interglacial cycles (Fig. 1b), the synchronicity of a few turbidites with millennial variability Heinrich stadials cannot be translated into convergent triggers in the deep ocean. Therefore, based on observations of disruptive turbidites at very low frequencies in general, and the lack of synchronicity of events in particular, it cannot be proven that global sea-level and climate changes (on orbital and millennial scales) are the primary forcing cause of slope instability and the triggering of turbidity currents in the Tore and nearby Rincão da Pomba basins, and the distal Tagus Abyssal Plain.

The earthquake-turbidite cause-effect relationship seems conceptually easy to postulate and demonstrate in areas of strong seismic activity and proximity to the earthquake source, where canyons are fed by continental shelf sensitive shaking sediments led to abyssal depths (e.g., Goldfinger et al., 2007; Mérindol et al., 2022; Bektaş et al., 2024). Although paleoseismicity reconstructions from turbidites are known to be associated with canyons and proximal to major earthquake sources in the southwest Portuguese passive margin (Lebreiro et al., 1997; Gràcia et al., 2010; Masson et al., 2011), ground-truth events at all three of our sites lack synchronicity and widespread concurrence, and cannot therefore be interpreted as paleoseismites. It is improbable that a single earthquake could destabilise the slopes of three morphologically independent and unconnected abyssal domains in this relatively large regional area, rendering these scenarios unlikely in paleoseismological terms (Sumner et al., 2013). Tectonically, the Tore seamounts represent the northern end of the Early Cretaceous aseismic Madeira-Tore Rise ridge, formed near the slow seafloor spreading Mid-Atlantic Ridge (Peirce and Barton, 1991). These two considerations lead us to rule out seismic shocks as an applicable external forcing mechanism to explain our turbidite sequences.

Assessment of sediment accumulation at sites prior to turbidite deposition – The intrinsic properties of the sediment, such as excess weight and pore pressure due to changing sedimentation rates, can induce sediment stress and subsequent slope instability in the deep sea. The potential amount of sediment available in situ prior to turbidite triggering can be inferred from sedimentation rate estimation (Fig. 2). Our data show that a higher accumulation rate in situ prior to placement of a given turbidite is not a necessary condition for either triggering or generating thicker turbidites. This is particularly verifiable at site MD13-3473, which is confined in the deep basin of the Tore seamounts and is undisturbed from resuspension and erosion of bottom currents, and where the turbidite record is therefore assumed to be hypothetically complete. Sites D219 and D11956, combining continental and submarine seamounts sediment sources, would, however, imply a more cautious approach. Consequently, our observations suggest that preconditioning or oversteepening by increased sediment accumulation is

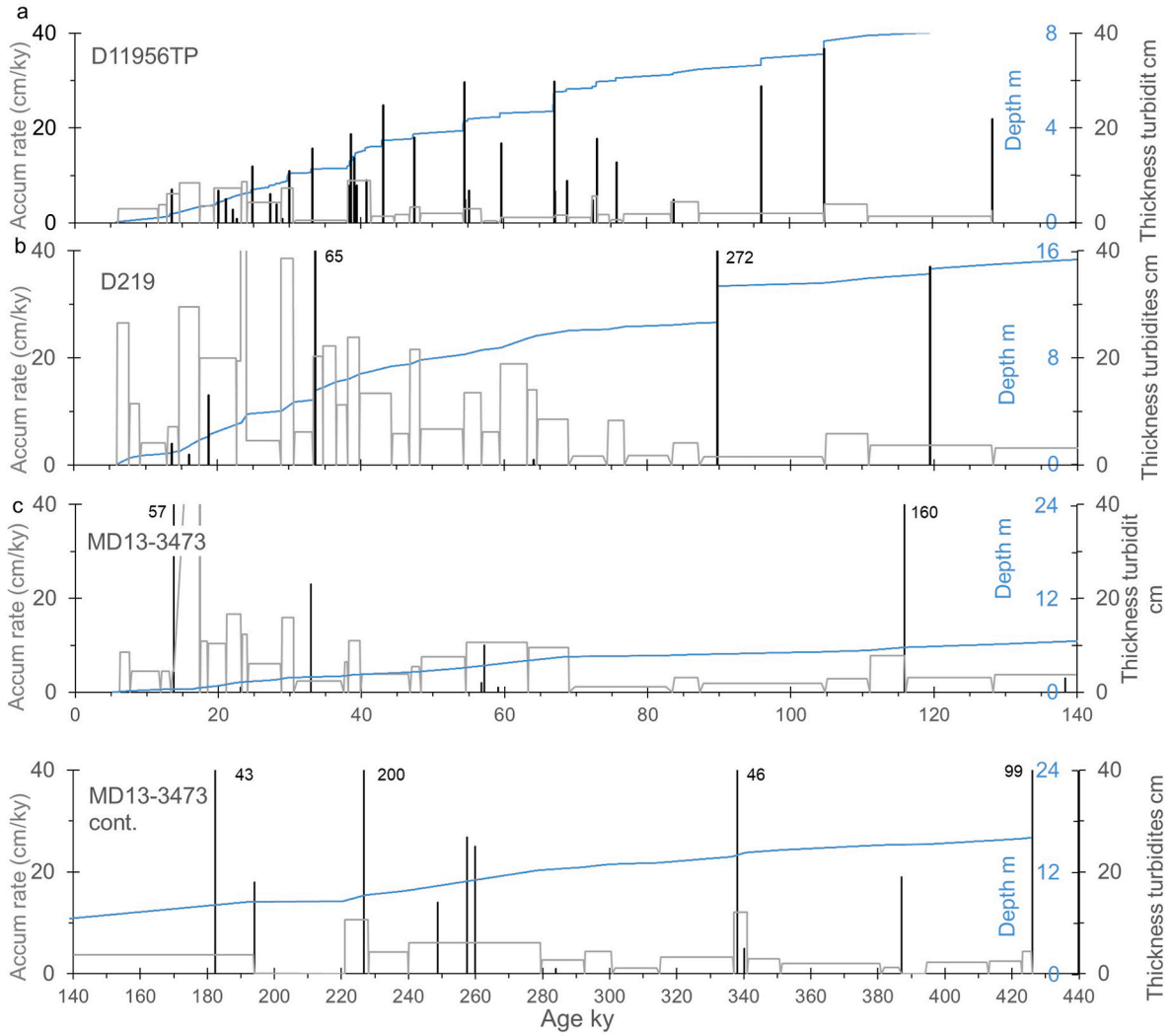

Fig. 2. Assessment of sediment accumulation at sites prior to turbidite deposition for cores D11956 T/P (a), D219/3P (b), and MD13-3473 (c, split into two panels). Sedimentation rate of hemipelagic sediment (grey rectangles and blue line) and thickness of turbidites (black vertical lines; small numbers next to vertical lines are turbidites with cm-thickness exceeding the Y-axis scale). (For interpretation of the references to colour in this figure legend, the reader is referred to the Web version of this article.)

unlikely to explain turbidite recurrence here. This is consistent with the findings of Urlaub et al. (2013), who reported delayed landslide failure thousands of years after increased sedimentation rates.

Since sea-level/climate, seismic forcing or rapid accumulation rates cannot explain the irregular pattern of turbidite occurrence in the three new offshore deep sea records, we now consider alternative mechanisms that could be at work, capable of triggering turbidity currents in the deep ocean.

3.2. Tides on the Tore seamounts

Tides may be potentially important in preconditioning failure of slopes in the Tore area through several mechanisms: (1) conversion of barotropic to baroclinic energy at depth by tidal forcing; (2) scattering of energy across the internal wave spectrum towards higher modes; (3) production of local resonantly generated trapped waves and Taylor column caps by low-frequency forcing; and (4) nonlinear rectified and amplified flow around the Tore seamounts by tide-slope interaction.

Conversion of barotropic to baroclinic tides - The effect of impinging oscillatory tidal flow on seamounts depends greatly on the seamount morphology (size, shape, and flank slope). We first focused on the flow dynamics along the edges and inside the Tore seamounts to determine how tides may promote energetic motions near the Tore slopes. We were concerned with i) the mean flow associated with tidal rectification and ii) mixing processes forced by internal tide generation and interaction with the Tore topography.

The interaction of tidal flow with seamounts is dependent on latitude, its incident wave frequency and local slope steepness. To assess the criticality of the response to topography we measured the steepness parameter (s/α; s being the topographic slope), where the critical slope of the internal tidal beams is $\alpha=((\omega^2-f_0^2)/(N^2-\omega^2))^{½}$ (f_0 is the local Coriolis parameter, N^2 is the buoyancy frequency squared, $\omega = 2\pi/T$ is the tidal frequency, and T is the tidal period). For frequencies above the local Earth rotation ($\omega>f_0$), if s/α is higher than 1, the baroclinic response to barotropic tidal forcing is in the supercritical regime, and higher baroclinic modes will likely be generated. For subcritical regimes ($s/\alpha < 1$), low modes are generated that are not efficient in producing enough shear. Although some interaction and energy transfer between modes is possible, the time scale for this spectral interaction is larger than that associated with the group velocity, which propagates the energy away from the generation point. Unless supercritical conditions are met, a transfer of barotropic tidal energy to small-scale turbulence is not expected. The agreement between the s/α parameter estimated from observations and the one estimated with model data is good (Fig. 3).

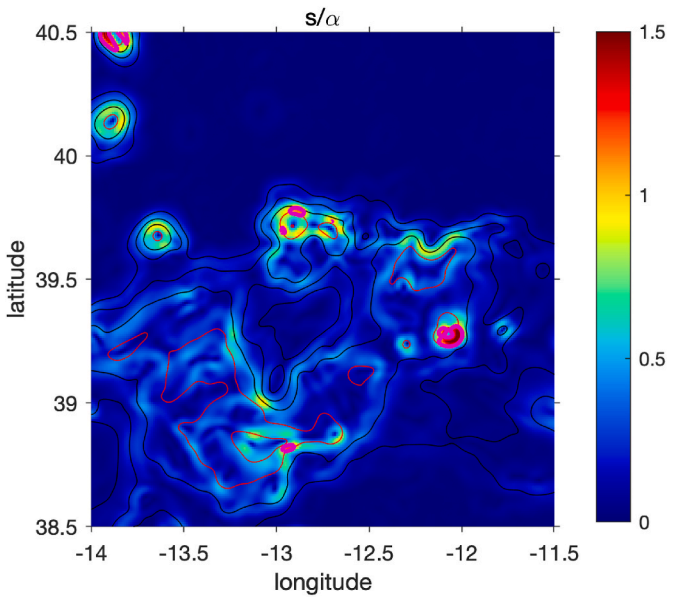

Fig. 3. Estimation of the slope criticality (s/α ratio) using model topography in the Tore seamounts area. Climatological hydrographic data are used to estimate N^2 (buoyancy frequency squared). The colour scale is saturated at s/α = 1.5. There are many critical and near critical values around the Tore seamounts. Supercritical values (s/α > 1) are contoured in magenta. Solid contours represent isobaths (black lines: 4, 4.5 and 5 km; red lines: 3 and 3.5 km). The real ocean topography (not shown) should have even steeper slopes and higher criticality. (For interpretation of the references to colour in this figure legend, the reader is referred to the Web version of this article.)

High values of s/α, including near critical and supercritical conditions, are present on the summit of the individual seamounts, especially along the northern flank of the Tore seamounts (Fig. 3). Inside the Tore seamounts the estimates are below the critical conditions. Other topographic features located in the vicinity of the Tore seamounts at distances not exceeding 1 to 3 mode 1 M_2 baroclinic wavelengths (we estimate the M2 mode 1 wavelength to be about 150 km) also support the hypothesis that baroclinic tides generated remotely may interact with the Tore seamounts. Turnewitsch et al. (2013) suggest that even in subcritical regimes, the orientation of the internal tidal beams may align parallel to the slope and induce velocity shear near the ground.

On the nearby Josephine seamounts, S of the Tore seamounts and SW of the Tagus Abyssal Plain, based on high-resolution temperature sensor moorings (water depths 2200–2900 m), a 100-fold increase in turbulence on the steepest (9.4°) and supercritical (α ≈ 0.4s) bottom slopes is reported to be associated with large nonlinear internal wave breaking, with strong variations in magnitude over relatively short distances of 3–5 km though (Van Haren et al., 2015). Waves steepen and break when the dominant internal wave phase speed matches the particle velocity (Van Haren et al., 2015) and the seamount slope angle approaches the characteristic slope of the internal waves (Lister, 1976). Accordingly, local features and the topographic configuration can induce significant flow-field and mirrored sediment distribution asymmetry (Lonsdale et al., 1972) in the interaction of internal tides with the bottom, and this is a determining factor in sediment mobilisation (Van Haren et al., 2015). Similar asymmetry is also evident in sediments deposited by turbidity currents on the eastern side of the Great Meteor seamount, South of the Azores islands in the Atlantic (von Stackelberg et al., 1979). At the Horizon guyot in the northern central Pacific, Lonsdale et al. (1972) propose that the interaction of internal tides with sediment-covered seamounts controls the inclination of eroding sediment slopes when the slope angle equals the inclination of internal tide energy flux. Likewise, they note that the seamount bed sediment appears to be swept upslope by accelerated tidal currents, contributing to slope erosion.

Scattering to higher energy modes - Scattering of internal waves is an efficient process for energy transfer between modes. Scattering over steep topography, especially convex slopes, may produce a flattening of the internal wave spectra with a flux of energy towards higher modes. More energy on higher modes (higher frequencies) implies a higher likelihood of turbulence that ultimately may affect the resuspension processes of the benthic layers around the Tore seamounts.

Internal wave generation converts barotropic to baroclinic energy in stratified water with variable seafloor bathymetry (Garrett and Kunze, 2007). An estimate of the available baroclinic energy indicates that a substantial part of the barotropic energy is converted to baroclinic higher modes, which produce significant interactions with the sharp topography of the Tore seamounts as seen in Fig. 4, even at very deep levels. Although the bulk of the energy is shown concentrated around the permanent pycnocline above −1500 m, part of it propagates downwards as expected along internal tide rays. In our simulations, we observe several rays that are rooted at the summits around Tore. Note that these peaks were classified as critical in the previous analysis (Fig. 3). However, we should note that this analysis is an approximation, as we are using a hydrostatic model. Higher-frequency internal waves may arise from the interaction of the baroclinic tide with topography, which we cannot estimate in this study. Near-inertial internal waves are also known to be relevant for the BBL dynamics and slope flows (Xie et al., 2023). Future studies should consider these dynamics.

Trapped waves and Taylor caps - At the Tore seamounts latitude, the inertial period (Tf = 2π/f) is approximately 18.8 h, implying that diurnal tides are subinertial ($\omega<f_0$) and may generate freely propagating topographic trapped waves (Lavelle and Mohn, 2010; Turnewitsch et al., 2013) around these seamounts. The amplitude of diurnal tides over the Tore seamounts is, however, rather small (below 0.1 m in the TPXO model). To predict the tendency of low-frequency forcing ($\omega<f_0$) to develop coherent time-mean flow structures such as trapped waves or Taylor caps on isolated topographic features, we use the Burger number ($S=NH/f_0L$) and the Rossby number ($Ro = U/Lf_0$) (where H is the water depth and L is a lateral length scale of the Tore seamounts; and N is the buoyancy frequency and f_0 is the Coriolis parameter as above), together with the fractional seamount height $\delta = h_{max}/H$ (where h_{max} is the height of the seamount and H is the water depth ~5000 m) (e.g, Lavelle and Mohn, 2010). By introducing climatological stratification data and certain intervals for h_{max} (~2500 m) and L (L = 100 km as the outer length of the whole seamount, and L ~ 20 km as the inner boundary of topographic features such as the small seamounts around the Tore), we estimate some intervals for these dimensionless dynamical scales: S = [0.3–2.3]; δ = 0.62; Ro = [0.005–0.01]. Assuming these limits, the Tore seamounts appear to have the potential to produce resonantly generated trapped waves and trapped Taylor column/caps, as otherwise shown in the cases of the nearby Seine and Sedlo seamounts in the Atlantic (White and Mohn, 2002), or the Fieberling and Caiwei guyots in the Pacific (Beckmann and Haidvogel, 1997; Brink, 1995; Guo et al., 2024). Guo et al. (2024) further suggest mesoscale perturbations from the upper layer to provide energy to excite trapped waves on the deep Pacific Caiwei guyot. Periodic forcing is capable of producing a strong wave response to resonant amplification (Beckmann, 1995). Seamount-trapped waves are therefore likely to lead to higher-frequency (diurnal) and high-amplitude fluctuations in current speed and direction on and around the summits of seamounts. These processes are relevant to the dynamics of sediment deposition and/or erosion; in many locations of the seamounts, the maximum total tidal current speed near the seafloor is higher than the threshold current speed (6–8 cm/s) needed for resuspension (Turnewitsch et al., 2013).

Non linear rectified flow - A final aspect of the circulation at seamounts caused by an impinging oscillatory flow is the generation of a steady unidirectional residual current (Lavelle and Mohn, 2010). Thus, we addressed the production of time-mean residual flows over topography by nonlinear rectification driven by both semidiurnal and diurnal

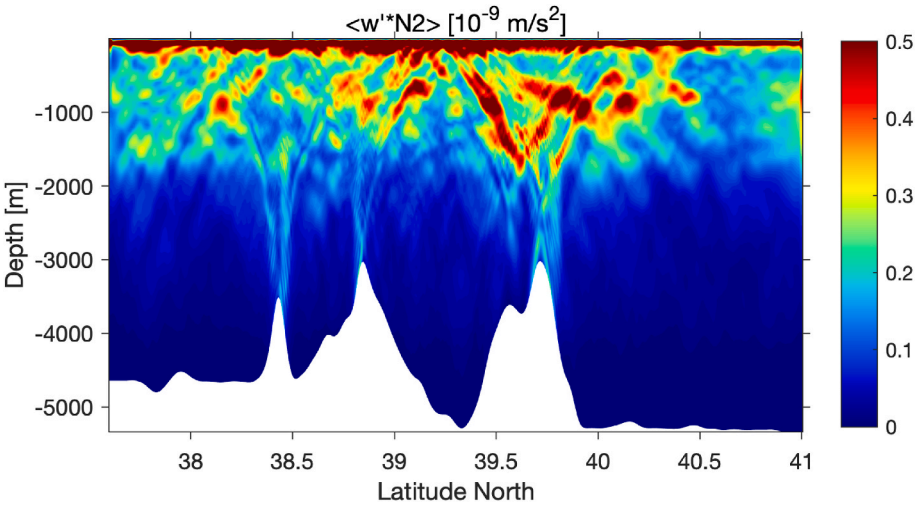

Fig. 4. Estimation of tidal energy conversion (from barotropic to baroclinic) w'N^2 (w' vertical velocity fluctuations; N^2 buoyancy frequency squared) in metres per second squared (m/s^2), averaged over the entire two-month simulation.

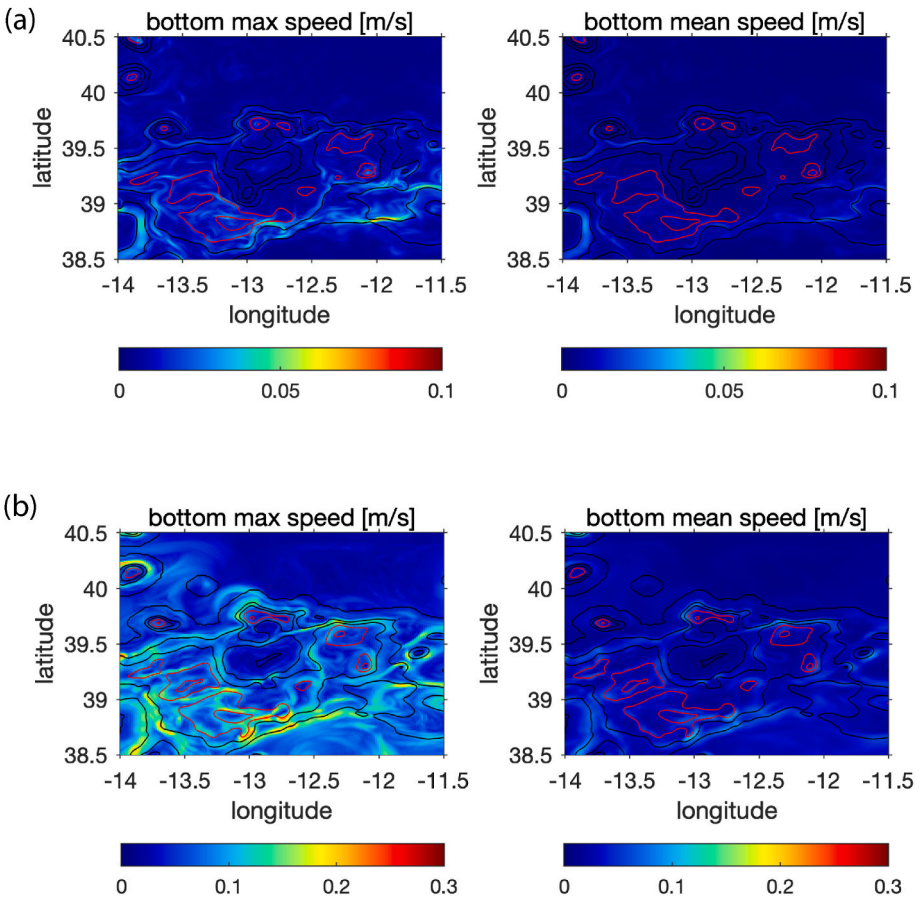

Fig. 5. Bottom flow magnitude (speed) maximum (left) and mean (right) for the entire two-month of the tidally-forced (a) and mesoscale (b) simulations. Solid contours represent isobaths (black lines: 4, 4.5 and 5 km; red lines: 3 and 3.5 km). Note the difference in colour scale between the tidal and mesoscale cases. (For interpretation of the references to colour in this figure legend, the reader is referred to the Web version of this article.)

tides. Fig. 5a shows the bottom time-mean flow (averaged over two months) produced by the interaction between tides and topography, with velocities rarely exceeding 2–3 cm/s. This flow is too small and may have contributions from both periodic trapped motions and background spurious numerical currents (see methods).

At the Fieberling Guyot, Beckman & Haidvogel (1997) show that rectification depends critically on the eddy fluxes balancing the time-mean downwelling over the seamount summit and upper flanks. Tidal rectification and amplification at the seamounts contribute significantly to the residual circulation (Brink, 1995; Turnewitsch et al., 2013). Residual flows can consequently reach substantial amplitudes with strong implications for sediment dynamics (White and Mohn, 2002). However,

in the case of Tore, the tidally driven time-mean rectified flow does not seem to be relevant. The maximum bottom velocities shown in Fig. 5b indicate that the maximum values can exceed the background flow by a large margin, reaching values above 5 cm/s in some places. These are mainly associated with periodic (5–12 day periodicities - not shown) trapped modes.

The several CTD casts collected in the Tore basin and around its periphery showed a strong homogenisation of the entire water column inside the Tore basin (Fig. 6) for depths below the −4300 m sills (Fig. 1). Such a level of mixing is much higher than that found at equivalent depths outside the Tore seamounts, where mixing is one to two orders lower, indicating that some specific mixing processes might occur inside the Tore basin. Note that the potential temperature of the Tore basin mixed water (station 60) is close to that of the lower level near the sill depth (station 59) in Fig. 6.

The casts obtained on the external part of the Tore seamounts exhibit a change in the slope of the potential temperature profile close to the bottom (Fig. 6). This may be an indication of slope flow. Using a simple scaling method (e.g., MacCready and Rhines, 1993) that relates the bottom layer height H_{bl}, the slope s, stratification N^2, and bottom velocity V, one can make a rough assessment of the velocities for the different stations. The bottom slope was estimated from the topography at the CTD cast position. Then temperature and salinity were used to estimate N^2. Applying the N^2 values shown in Fig. 6 to estimate $V=H_{bl}*N^2*s/f$ (f for local Coriolis), the velocities obtained are in the range of 2–5 cm/s. Despite the simplicity of the scaling, the values agree in terms of magnitude with the estimates of bottom currents produced by the model at the Tore seamounts. This flow may complement other processes triggering turbidity currents. We see that these values are even higher in the case of the mesoscale simulations.

3.3. Interaction of intermediate mesoscale eddies with the Tore seamounts

In addition to the tidally driven dynamics discussed above (3.2), intermittent interaction of eddies with topography may favour intense slope flows and thereby develop the conditions conducive to significant downslope turbidity currents.

The seamounts along the paths of the Mediterranean Overflow Water (MOW) are known to be places of intense ocean eddy activity (Richardson et al., 2000). The Tore seamounts are located in an area of considerable transit of Mediterranean Overflow Water eddies (Meddies) (Ambar et al., 2008), and have their main salinity signature roughly between −500 m to −1500 m. Previous work on the census of drifter tracks trapped by Meddies shows that the probability of Meddy–Tore encounters in a time-window of a few years is significant (Richardson et al., 2000; Barbosa-Aguiar et al., 2013). Although a large portion of Meddies tend to separate off Cape S. Vincent, a substantial number (10/year) are generated close to the Estremadura Spur and drift off the slope along a corridor that crosses the latitudes of the Tore (Fig. 7). The trajectories of a large population of Meddies generated in the Gulf of Cadiz, submarine canyons, seamounts and the Extremadura Spur were traced around the Iberian margin, while running an eddy-tracking algorithm for a high-resolution 20-year simulation of Meddy formation and propagation, identifying salinity and density anomalies (Barbosa-Aguiar et al., 2013). These modelled Meddies migrated and impacted the Tore seamounts region (Fig. 7), where their trajectories showed signs of being deflected around the Tore summits, and vertically reached the approximate depth of the Tore seamounts summit at −2200 m water depth (Barbosa-Aguiar et al., 2013). Therefore, the likelihood of Meddy–Tore seamount interactions at present appears to be high (e.g., Richardson et al., 2000; Barbosa-Aguiar et al., 2013), and the downward influence of eddies colliding with bottom topography is not uncommon.

We examined the mesoscale structure and bottom flow of a realistic circulation model with a resolution of 1 km covering the Tore area. During the available 6-month period, there were no clear examples of a 'canonical Meddy'-Tore encounter. However, there were several instances of upper-ocean mesoscale structures around the Tore area that coincided with bottom-trapped flows. Fig. 7a shows the model's synoptic salinity distribution at −1000 m, where high salinity structures ('Meddies' in the broad sense) are present. The Tore is located at the northwestern end of the domain, and a cyclonic, high-salinity core structure is observed to the north at this time, surrounded by swirling, low-salinity arms that can be classified as a shallow, cyclonic 'Meddy' (see Barbosa-Aguiar et al., 2013). Over the Tore seamounts, a salinity front is visible, produced by a northward-protruding 'mushroom-like' deformed vortex pair. The corresponding vertical distribution of zonal velocities (quasi-cross-section flow) along the section marked by the blue line is shown in Fig. 7b.

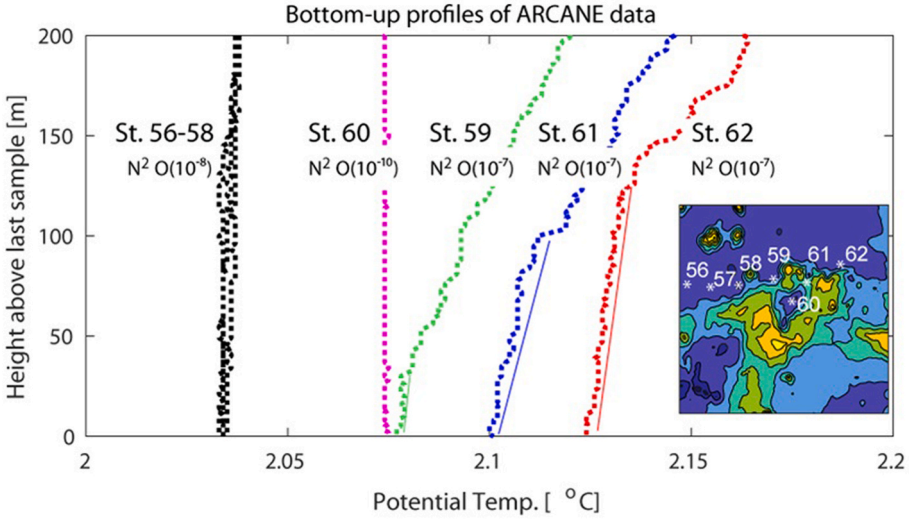

Fig. 6. Mixed layer inside and outside the Tore seamounts based on bottom temperature profiles (profiles are plotted bottom-up). CTD data were collected as close as possible to the bottom. The y-axis refers to the height above the deepest sample depth. Profiles are positioned in the abyss (black lines), inside the Tore seamounts (magenta; station 60), and over the Tore slopes/sill (green, blue, red). Solid lines show the possible depth of the bottom mixed layer associated with residual flows (see text). The numbers indicate the approximate value of stratification (buoyancy frequency squared, N^2) for the different stations computed for the last 200 m. The inset illustrates the position of stations above topography. (For interpretation of the references to colour in this figure legend, the reader is referred to the Web version of this article.)

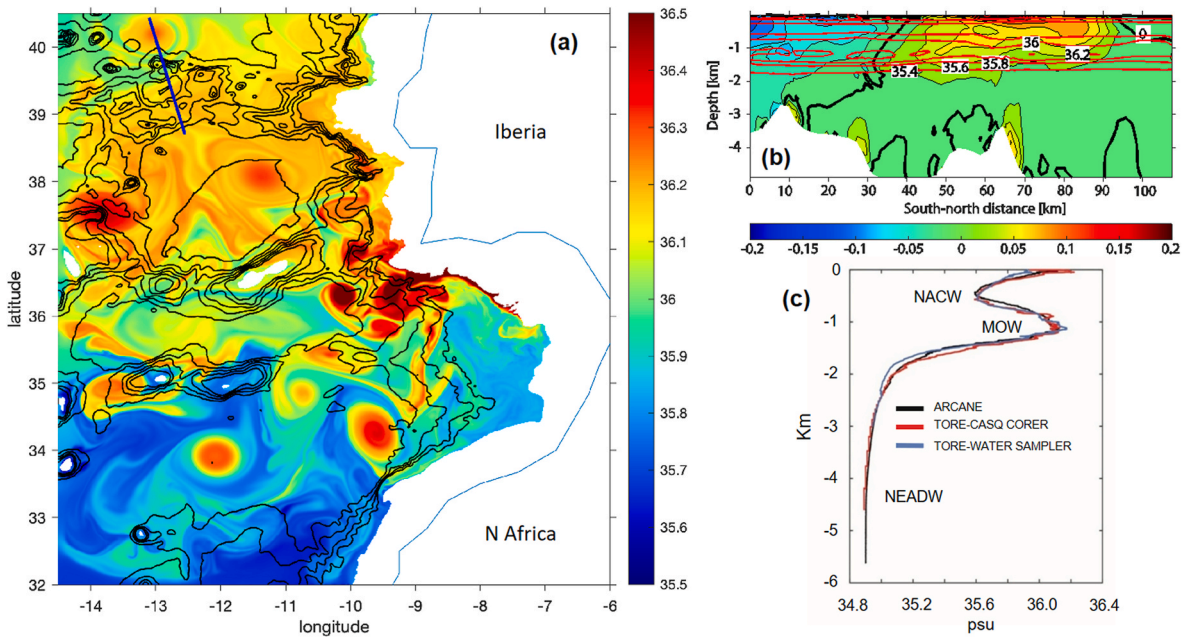

Fig. 7. Mesoscale simulation. (a) Instantaneous salinity field at a depth of −1000 m. The Tore is located in the north-west corner of the domain. The solid black contours represent isobaths (3, 3.5, 4, 4.5 and 5 km). (b) Vertical section of zonal velocity (positive values [m/s] indicate eastward flow) along the south-north section (blue line), as shown in (a). The contours are at 2 cm/s intervals, with the bold black line indicating zero velocity. The red lines show the vertical salinity distribution (from 35.2 to 36.2 in increments of 0.2). The bottom trapped flow features on the edges of the eddy reach values of 6–8 cm/s. (c) Vertical salinity profile from three CTDs deployed in the interior of the Tore seamount basin (site MD13-3473) showing Mediterranean Outflow Water (MOW) at depths between −600 and −1200 m. The other water masses in the profile are North Atlantic Central Water (NACW) and Northeast Atlantic Deep Water (NEADW) (van Aken, 2000a, 2000b). (For interpretation of the references to colour in this figure legend, the reader is referred to the Web version of this article.)

We observe that velocity structures in the upper ocean are generally more pronounced than salinity structures. However, the velocity signature becomes much weaker below −2000 m. Conversely, we observe localised flows on the seamount slopes that can reach velocities of up to 6 cm/s.

Mesoscale structures in the upper ocean may be associated with seamount-trapped flows. However, this association is not straightforward (e.g., Jiang et al., 2021, for a review). In our particular case, the advection of deep fluid parcels across the isobaths by upper ocean vortices due to constraints on potential vorticity conservation, seems especially important (e.g., Herbette et al., 2003). There is also a number of studies reporting the influence of surface structures on deep sea seamounts via the excitation of topographic Rossby Waves (see, e.g., Guo et al., 2020; Wang et al., 2021; Shu et al., 2022).

We have produced the same statistics for the bottom flow (maximum and mean over a six-month period), which are presented in Fig. 5. As can be seen, the mean flow (which may be contaminated by spurious numerical currents to some degree) is much lower than the maximum. This suggests that mesoscale, event-like flows dominate other modes of lower-frequency circulation. Conversely, it is interesting to note that mesoscale bottom flows are significantly larger than those tidally driven (note the difference in scale when comparing the figures). Mean mesoscale bottom flows may reach 0.1 m/s around the Tore summits, with maximum speeds of up to 0.2 m/s being registered.

Eddies have been observed down to depths as great as −4200 m in the Kyushu-Palau Ridge in the North Pacific (Andres et al., 2019). It is expected that energy will be transferred from mesoscale eddies to internal waves, turbulence, mixing and dissipation in regions of rough topography in the deep ocean (Liang and Thurnherr, 2012; Löb et al., 2020), such as the Iberian margin. In particular, Meddies are plausible candidates for such interactions because of their depth levels and frequent encounters with topography (Cenedese et al., 2005; Barbosa-Aguiar et al., 2013).

There is insufficient information on the depth range of eddies in the real ocean, or on how they interact with topography (Bashmachnikov et al., 2009; Andres et al., 2019; Löb et al., 2020). Scaled models of eddies comparable in size to Meddies found that eddy collisions occur in several ways (Cenedese, 2002). One particularly interesting feature is the development of toroidal-like circulation, known as “streamers” (Cenedese, 2002). Streamers are strong, slope-trapped flows that develop around seamounts as a result of eddy collisions. The direction of streamers depends on the incidence angle of the eddy collision, and they can be as intense as the eddies themselves. Previous analysis of several Meddy–seamount collisions (Barbosa-Aguiar et al., 2013) (not specifically on Tore) revealed that streamers are a common feature in Meddy–seamount interactions. Very high-resolution simulations of eddy–seamount interactions have also shown nearly balanced flows colliding and triggering the development of high-frequency internal waves (Dewar and Hogg, 2010). While no such study has been conducted for Meddies, one could expect the collisions to promote intermittent higher-frequency motions together with streamers (Löb et al., 2020).

As the results of our models only cover a very short period, it is not possible to conduct a consistent analysis of the eddy field. However, they already suggest that mesoscale flows may be even more important than tidally driven flows (Fig. 7). In our simulation, we did not detect any canonical Meddy (i.e., an isolated, unipolar vortex with a negative vorticity and a high-salinity core, intensified at around −1200 m depth). Nevertheless, it has previously been demonstrated (e.g., Aguiar et al., 2013) that the eddy field produced by the Mediterranean outflow includes a rich spectrum of vortices with different polarities, depth ranges, and modes of interaction that can be relevant in eddy-topography interactions. In this respect, ’Meddies’ in the broad sense must be considered in future studies of mesoscale flows.

3.4. Oceanographic processes during glacial periods

The extent to which the interaction of Meddies with topography has

been different in the past requires additional analysis. Stronger, deeper Meddies may have been more frequent in some periods in the recent past, as reported in a time series over the last 20 years, albeit with irregular periodicity (Siedler et al., 2005). If internal wave activity is, in theory, favoured by ocean stratification (Polzin et al., 1997) and glacial periods have supposedly enhanced deep salinity-driven stratification (Adkins and Pasquero, 2004; Wilmes et al., 2019), cold periods would be more prone to the generation of internal waves as a consequence of intermittent Meddies. Several studies have indeed shown an increase in Mediterranean outflow during glacial stages and cold millennial events (Cacho et al., 2006; Voelker et al., 2006; Rogerson et al., 2010; Lebreiro et al., 2018), but the formation and intensity of the Meddies in the Atlantic Iberian margin have not been correlated to specific sea-level/climate stages.

Egbert and Ray (2001) pointed out the often neglected important interaction between internal tides and ocean stratification. Model studies suggested that the last glacial (sea-level lowered by ~130 m; Lambeck et al., 2014) led to two times enhanced tidal amplitudes of global semidiurnal tides (M_2) in the North Atlantic, and increased dissipation in the deep ocean (a significant 30 % M_2 energy dissipation occurs in the deep ocean; 10 % below −1000 m) with reduced stratification, although the authors acknowledge that stratification is not well constrained in the models (Egbert et al., 2004) and abyssal tidal dissipation rates are relatively insensitive to changes in hydrography (Wilmes and Green, 2014).

On the other hand, the internal thermohaline structure of the deep ocean still contains caveats not fully resolved, such as the more salinity-stratified glacial ocean compared to today's temperature-driven stratification, supported by salinity contrasts in the glacial shoaling boundaries of different North or South-sourced water masses and kinks in the density profiles (Adkins, 2013). Adkins (2013) cites the MIS 5–MIS 4 transition as a prime example of increasing deep-ocean stratification. However, our records from the Tore and Rincão da Pomba basins show no turbidites during this transition, except for those in the Tagus AP (Fig. 1). This is consistent with evidence suggesting that under current global warming, an 8 % increase in energy conversion to high-mode internal tides and near-bottom stratification intensification is expected by the end of the 21st century (Yang et al., 2024).

4. Concluding remarks

Far from continental margins, the MD13-3473 non-periodic turbidite time series exhibit a lack of consistency associated with (sub)orbital and millennial (cold glacial/stadial or warm interglacial/interstadial) time scales, deviating from predictable mechanisms driven by any regular climatic forcing. It also shows no association with excess accumulation rates and no verifiable relationship with seismic shaking. D219/3P and D11956 T/P exhibit minor climatic similarities, likely due to the interposed sediment input from continental sources.

Potential oceanic mechanisms are identified and simulated for triggering turbidity currents in the deep ocean, potentially affecting the stability of critical seamount slopes and sediments, away from the continental margin. The contrast of our findings with continental margin studies underscore the uniqueness of deep-ocean mechanisms.

The tidal conversion estimates shown here suggest that although most of the internal tide activity is concentrated in the upper ocean (thermocline and above), a significant portion of the energy is produced at the summits of the Tore system. Internal waves can promote intense mixing and turbulence regardless of depth in well-mixed abyssal zones, with occasional breaking, inducing the disturbance of sediments. Hence, the influence of internal tides, even with small amplitudes, cannot be dismissed as a potential mechanism and should be considered further in future modelling studies that also include non-hydrostatic effects and higher resolution topography.

It appears that the Tore seamounts are rather susceptible to the mechanisms analysed above (barotropic to baroclinic energy conversion; internal wave–topography interactions: trapped waves, rectified flow, slope flow; and Meddy–seamount collision). Meddy–seamount (and here we refer to 'Meddies' in the broad sense) collision is probably the most likely candidate to generate bottom velocity stresses sufficiently strong to trigger turbidity currents. Although none of the processes alone may induce very high bottom flow, a combination of processes in peak and phase amplitudes with particularly strong Meddy events can act together to produce exceptional non-periodic triggers in vulnerable areas of the real ocean, and explain the low-frequency, non-periodic, climate-independent turbidite records observed in the deep Iberian margin.

It remains to be resolved whether the non-periodic pattern and low frequency of turbidites in these three unique deep sea series would require an exceptional combination of intermittent physical oceanographic processes, including the interaction of concurrent high-frequency internal waves (tidal and near inertial), mesoscale eddies and currents (Turnewitsch et al., 2013; Löb et al., 2020), megatides (Griffiths and Peltier, 2008, 2009) or periods of higher-frequency megatides, to trigger extreme turbidity currents.

CRediT authorship contribution statement

Susana M. Lebreiro: Writing – review & editing, Writing – original draft, Visualization, Validation, Supervision, Resources, Project administration, Methodology, Investigation, Funding acquisition, Formal analysis, Data curation, Conceptualization. **Álvaro Peliz:** Writing – review & editing, Writing – original draft, Visualization, Validation, Methodology, Investigation, Formal analysis, Conceptualization. **Laura Antón:** Writing – review & editing, Validation, Resources, Methodology, Investigation, Formal analysis, Data curation. **Sílvia Nave:** Writing – review & editing, Visualization, Resources, Project administration, Investigation, Funding acquisition, Data curation, Conceptualization. **M. Isabel Reguera:** Writing – review & editing, Methodology, Formal analysis. **Rocío Lozano-Luz:** Methodology, Formal analysis. **Claire Waelbroeck:** Writing – review & editing, Methodology, Formal analysis. **Simon Crowhurst:** Writing – review & editing, Methodology, Formal analysis. **Belen Martrat:** Writing – review & editing, Project administration, Funding acquisition. **Jordi F. Lopez:** Validation, Methodology, Formal analysis. **Raphaël Hebert:** Validation, Methodology, Formal analysis. **Alejandra Lopez-Rodriguez:** Writing – review & editing, Methodology.

Declaration of competing interest

The authors declare that they have no known competing financial interests or personal relationships that could have appeared to influence the work reported in this paper.

Acknowledgements

This work was performed within the framework of the TORE-5deg (CTM 2017-84113-R, Ministerio de Economia, Industria y Competitividad) and IBCC-Shack (PID2022-137665NB-I00, AEI/10.13039/501100011033/FEDER, UE, Ministerio de Ciencia e Innovación) Spanish projects. S.M.L. benefitted from a 6-month sabbatical grant (PRX 18/00268) of the Spanish Ministerio de Educación, Cultura y Deporte and the Godwin Laboratory for Paleoclimate Research (GLPR), Department of Earth Sciences, University of Cambridge, UK. Previous work in core D219 was developed during TMR-*Marie Curie*-ERBFMBICT983111 and PRAXIS XXI/BDP/19000/98 grants (S.M.L.) at the Instituto Geológico e Mineiro of Portugal. A.L.-R. acknowledges grant JAE INT_23_01648 (CSIC, Ministerio de Ciencia e Innovación).

The British Ocean Sediment Core Research Facility of the UK is thanked for supporting the Itrax-XRF core scanning data collection of D11956 trigger and piston cores, as part of the BOSCORF Legacy data program. IGME-CSIC provided intramural funds for XRF-scan

measurements of core MD13-3473 at the University of Barcelona. The recovery of calypso core MD13-3473 and the Tore CTD-data was financially supported by the EU project EUROFLEETS Grant agreement n° 228344 (S.N.) through access to ship-time on Marion Dufresne, operated by the French Polar Institute Paul-Émile Victor (IPEV). Four AMS ^{14}C dates of core D11956 T/P were paid for by an intramural project (INETI, 2007). David Hodell and the GLPR provided part of the MD13-3473 isotope data.

A number of the authors of this paper are part of CSIC-HUBs (Connections CSIC) - Geosciences for a Sustainable Planet.

Appendix A. Supplementary data

Supplementary data to this article can be found online at https://doi.org/10.1016/j.dsr.2025.104557.

Data availability

All the data included in this article are in the Supplementary Material, and data sets (Lebreiro et al., 2025) in PANGAEA-Data Publisher for Earth & Environmental Science (www.pangaea.de).

References

Adkins, J.F., 2013. The role of deep ocean circulation in setting glacial climates. Paleoceanography 28 (3), 539–561. https://doi.org/10.1002/palo.20046.

Adkins, J.F., Pasquero, C., 2004. Deep ocean overturning-then and now. Science 306 (5699), 1143–1144. https://doi.org/10.1126/science.1105531.

Allin, J.R., Hunt, J.E., Talling, P.J., Clare, M.A., Pope, E., Masson, D.G., 2016. Different frequencies and triggers of canyon filling and flushing events in nazaré canyon, offshore Portugal. Mar. Geol. 371, 89–105. https://doi.org/10.1016/j.margeo.2015.11.005.

Allin, J.R., Hunt, J.E., Clare, M.A., Talling, P.J., 2017. Eustatic sea-level controls on the flushing of a shelf-incising submarine canyon. GSA Bulletin 130 (1–2), 222–237. https://doi.org/10.1130/B31658.1.

Ambar, I., Serra, N., Neves, F., Ferreira, T., 2008. Observations of the mediterranean undercurrent and eddies in the Gulf of Cadiz during 2001. J. Mar. Syst. 71, 195–220. https://doi.org/10.1016/j.jmarsys.2007.07.003.

Andres, M., Siegelman, M., Hormann, V., Musgrave, R.C., Merrifield, S.T., Rudnick, D.L., et al., 2019. Eddies, topography, and the abyssal flow by the kyushu-palau ridge near velasco reef. Oceanography (Wash. D. C.) 32, 46–55. https://doi.org/10.5670/oceanog.2019.410.

Azpiroz-Zabala, M., Cartigny, M.J.B., Talling, P.J., Parsons, D.R., Sumner, E.J., Clare, M. A., et al., 2017. Newly recognized turbidity current structure can explain prolonged flushing of submarine canyons. Sci. Adv. 3 (10). https://doi.org/10.1126/sciadv.1700200.

Barbosa-Aguiar, A., Peliz, A., Xavier, C., 2013. A census of Meddies in a long-term high-resolution simulation. Prog. Oceanogr. 116, 80–94. https://doi.org/10.1016/j.pocean.2013.06.016.

Bashmachnikov, I., Mohn, C., Pelegrí, J.L., Martins, A., Jose, F., Machín, F., et al., 2009. Interaction of mediterranean water eddies with sedlo and seine seamounts, subtropical northeast Atlantic. Deep sea research - part II top. Stud. Oceanogr. 56, 2593–2605. https://doi.org/10.1016/j.dsr2.2008.12.036.

Beckmann, A., 1995. Numerical modeling of time-mean flow at isolated seamounts. In: Müller, Peter, Henderson, Diane, Sp, S.O.E.S.T. (Eds.), Topographic Effects in the Ocean. Proceedings 'Aha Huliko'A, Hawaiian Winter Workshop, Univ. Hawaii at Manoa, pp. 57–66. https://doi.org/10.1029/96JC03414. Publ. 1995.

Beckmann, A., Haidvogel, D.B., 1997. A numerical simulation of flow at fieberling guyot. J. Geophys. Res. 102 (C3), 5595–5613. https://doi.org/10.1029/96JC03414.

Bektaş, Z., Avşar, U., Ribot, M., Klinger, Y., Jónsson, S., 2024. Seismo-turbidites reveal locations of major earthquakes during the past millennium in the gulf of Aqaba, southern Dead Sea fault. Earth Planet Sci. Lett. 629, 118595. https://doi.org/10.1016/j.epsl.2024.118595.

Bell Jr., T.H., 1975. Topographically generated internal waves in the open ocean. J. Geophys. Res. 80 (3), 320–327. https://doi.org/10.1029/JC080i003p00320.

Bond, G., Broecker, W., Johnsen, S., McManus, J., Labeyrie, L., Jouzel, J., Bonani, G., 1993. Correlations between climate records from North Atlantic sediments and Greenland ice. Nature 365 (6442), 143–147. https://doi.org/10.1038/365143a0.

Brink, K.H., 1995. Tidal and lower frequency currents above fieberling guyot. J. Geophys. Res.: Oceans 100 (C6), 10817–10832. https://doi.org/10.1029/95JC00998.

Cacho, I., Shackleton, N., Elderfield, H., Sierro, F.J., Grimalt, J.O., 2006. Glacial rapid variability in deep-water temperature and δ^{18}O from the Western Mediterranean Sea. Quat. Sci. Rev. 25 (23–24), 3294–3311. https://doi.org/10.1016/j.quascirev.2006.10.004.

Carter, L., Gavey, R., Talling, P.J., Liu, J.T., 2014. Insights into submarine geohazards from breaks in subsea telecommunication cables. Oceanography (Wash. D. C.) 27 (2), 58–67. https://doi.org/10.5670/oceanog.2014.40.

Cenedese, C., 2002. Laboratory experiments on mesoscale vortices colliding with a seamount. J. Geophys. Res.: Oceans 107 (C6). https://doi.org/10.1029/2000JC000599, 6-1.

Cenedese, C., Adduce, C., Fratantoni, D.M., 2005. Laboratory experiments on mesoscale vortices interacting with two islands. J. Geophys. Res.: Oceans 110 (C9). https://doi.org/10.1029/2004JC002734.

Dansgaard, W., Johnsen, S.J., Clausen, H.B., Dahl-Jensen, D., Gundestrup, N.S., Hammer, C.U., et al., 1993. Evidence for general instability of past climate from a 250-kyr ice-core record. Nature 364 (6434), 218–220. https://doi.org/10.1038/364218a0.

Dewar, W.K., Hogg, A.M., 2010. Topographic inviscid dissipation of balanced flow. Ocean Model. 32 (1–2), 1–13. https://doi.org/10.1016/j.ocemod.2009.03.007.

Dypvik, H., Harris, N.B., 2001. Geochemical facies analysis of fine-grained siliciclastics using Th/U, Zr/Rb and (Zr+ Rb)/Sr ratios. Chem. Geol. 181 (1–4), 131–146. https://doi.org/10.1016/S0009-2541(01)00278-9.

Egbert, G.D., Ray, R.D., 2001. Estimates of M2 tidal energy dissipation from TOPEX/Poseidon altimeter data. J. Geophys. Res. 106 (C10), 22475–22502. https://doi.org/10.1029/2000JC000699.

Egbert, G.D., Ray, R.D., Bills, B.G., 2004. Numerical modeling of the global semidiurnal tide in the present day and in the last glacial maximum. J. Geophys. Res.: Oceans 109 (C3). https://doi.org/10.1029/2003JC001973.

Felden, J., Möller, L., Schindler, U., Huber, R., Schumacher, S., Koppe, R., Diepenbroek, M., Glöckner, F.O., 2023. PANGAEA – Data Publisher for Earth & Environmental Science. Sci. Data 10 (1), 347. https://doi.org/10.1038/s41597-023-02269-x.

Gamboa, D., Omira, R., Terrinha, P., 2021. A database of submarine landslides offshore west and southwest iberia. Sci. Data 8 (1), 185. https://doi.org/10.1038/s41597-021-00969-w.

Garrett, C., Kunze, E., 2007. Internal tide generation in the deep ocean. Annu. Rev. Fluid Mech. 39 (1), 57–87. https://doi.org/10.1146/annurev.fluid.39.050905.110227.

Goldfinger, C., Morey, A.E., Nelson, C.H., Gutiérrez-Pastor, J., Johnson, J.E., Karabanov, E., et al., 2007. Rupture lengths and temporal history of significant earthquakes on the offshore and north coast segments of the Northern San Andreas Fault based on turbidite stratigraphy. Earth Planet Sci. Lett. 254 (1–2), 9–27. https://doi.org/10.1016/j.epsl.2006.11.017.

Gràcia, E., Vizcaino, A., Escutia, C., Asioli, A., Rodes, A., Pallas, R., et al., 2010. Holocene earthquake record offshore Portugal (SW iberia): testing turbidite paleoseismology in a slow-convergence margin. Quat. Sci. Rev. 29 (9–10), 1156–1172. https://doi.org/10.1016/j.quascirev.2010.01.010.

Griffiths, S.D., Peltier, W.R., 2008. Megatides in the Arctic Ocean under glacial conditions. Geophys. Res. Lett. 35 (8). https://doi.org/10.1029/2008GL033263.

Griffiths, S.D., Peltier, W.R., 2009. Modeling of polar ocean tides at the last glacial maximum: Amplification, sensitivity, and climatological implications. J. Clim. 22 (11), 2905–2924. https://doi.org/10.1175/2008JCLI2540.1.

Grootes, P.M., Stuiver, M., White, J.W.C., Johnsen, S., Jouzel, J., 1993. Comparison of oxygen isotope records from the GISP2 and GRIP Greenland ice cores. Nature 366 (6455), 552–554. https://doi.org/10.1038/366552a0.

Gutierrez-Pastor, J., Goldfinger, C., Nelson, C., Johnson, J., Escutia, C., Eriksson, A., et al., 2009. Earthquake control of Holocene turbidite frequency confirmed by hemipelagic sedimentation chronology on the cascadia and northern California active Continental margins. J. Sediment. Res. B Stratigr. Global Stud.: An International Journal of SEPM (Society for Sedimentary Geology) 92, 179–197. https://doi.org/10.2110/sepmsp.092.179.

Guo, B., Shu, Y., Wang, W., He, G., Liang, Q., Zhang, D., et al., 2024. Observations of intermittent seamount-trapped waves and topographic rossby waves around the slope of a low-latitude deep seamount. J. Phys. Oceanogr. 54 (1), 281–299. https://doi.org/10.1175/JPO-D-22-0121.1.

Guo, B., Wang, W., Shu, Y., He, G., Zhang, D., Deng, X., et al., 2020. Observed deep anticyclonic cap over caiwei guyot. J. Geophys. Res.: Oceans 125 (10), e2020JC016254.

Heijnen, M.S., Mienis, F., Gates, A.R., Bett, B.J., Hall, R.A., Hunt, J., et al., 2022. Challenging the highstand-dormant paradigm for land-detached submarine canyons. Nat. Commun. 13 (1), 3448. https://doi.org/10.1038/s41467-022-31114-9.

Herbette, S., Morel, Y., Arhan, M., 2003. Erosion of a surface vortex by a seamount. J. Phys. Oceanogr. 33 (8), 1664–1679.

Hodell, D., Lourens, L., Crowhurst, S., Konijnendijk, T., Tjallingii, R., Jiménez-Espejo, F., et al., 2015. A reference time scale for site U1385 (shackleton site) on the SW iberian margin. Global Planet. Change 133, 49–64. https://doi.org/10.1016/J.GLOPLACHA.2015.07.002.

Hunt, J., Talling, P.J., Clare, M., Jarvis, I., Wynn, R.B., 2014. Long-term (17 Ma) turbidite record of the timing and frequency of large flank collapses of the Canary Islands. G-cubed 15. https://doi.org/10.1002/2014GC005232.

Jerolmack, D.J., Paola, C., 2010. Shredding of environmental signals by sediment transport. Geophys. Res. Lett. 37 (19). https://doi.org/10.1029/2010GL044638.

Jiang, X., Dong, C., Ji, Y., Wang, C., Shu, Y., Liu, L., et al., 2021. Influences of deep-water seamounts on the hydrodynamic environment in the Northwestern Pacific Ocean. J. Geophys. Res.: Oceans 126, e2021JC017396. https://doi.org/10.1029/2021JC017396.

Knudson, K., Hendy, I.L., 2009. Climatic influences on sediment deposition and turbidite frequency in the Nitinat Fan, British Columbia. Mar. Geol. 262, 29–38. https://doi.org/10.1016/j.margeo.2009.03.002.

Lambeck, K., Rouby, H., Purcell, A., Sun, Y., Sambridge, M., 2014. Sea level and global ice volumes from the Last Glacial Maximum to the Holocene. Proc. Natl. Acad. Sci. 111 (43), 15296–15303. https://doi.org/10.1073/pnas.1411762111.

Lavelle, J.W., Mohn, C., 2010. Motion, commotion, and biophysical connections at deep Ocean seamounts. Oceanography (Wash. D. C.) 23 (1), 90–103. https://doi.org/10.5670/oceanog.2010.64.
Lebreiro, S.M., 1995. Sedimentation History off Iberia: Tore Seamount, Tagus and Horseshoe Abyssal Plains. Doctoral dissertation, University of Cambridge.
Lebreiro, S.M., Antón, L., Reguera, M.I., Marzocchi, A., 2018. Paleoceanographic and climatic implications of a new mediterranean outflow branch in the southern Gulf of Cadiz. Quat. Sci. Rev. 197, 92–111. https://doi.org/10.1016/j.quascirev.2018.07.036.
Lebreiro, Susana Martin, Antón López, Laura, Reguera, Isabel, Lozano, Rocio, 2025a. Accumulation rate of sediment core D219/3P [dataset]. PANGAEA. https://doi.org/10.1594/PANGAEA.971124.
Lebreiro, Susana Martin, Antón López, Laura, Reguera, Isabel, Lozano, Rocio, 2025b. Accumulation rate of sediment core D11956TC/P [dataset]. PANGAEA. https://doi.org/10.1594/PANGAEA.971123.
Lebreiro, Susana Martin, Antón López, Laura, Reguera, Isabel, Lozano, Rocio, 2025c. Accumulation rate of sediment core MD13-3473 [dataset]. PANGAEA. https://doi.org/10.1594/PANGAEA.971125.
Lebreiro, Susana Martin, Antón López, Laura, Reguera, Isabel, Lozano, Rocio, 2025d. Ca/Ti ratio of sediment core D219-3P [dataset]. PANGAEA. https://doi.org/10.1594/PANGAEA.971117.
Lebreiro, Susana Martin, Antón López, Laura, Reguera, Isabel, Lozano, Rocio, 2025e. Ca/Ti ratio of sediment core D11956TC/P [dataset]. PANGAEA. https://doi.org/10.1594/PANGAEA.971118.
Lebreiro, Susana Martin, Antón López, Laura, Reguera, Isabel, Lozano, Rocio, 2025f. Ca/Ti ratio of sediment core MD03-2698 [dataset]. PANGAEA. https://doi.org/10.1594/PANGAEA.971119.
Lebreiro, Susana Martin, Antón López, Laura, Reguera, Isabel, Lozano, Rocio, 2025g. Ca/Ti ratio of sediment core MD13-3473 [dataset]. PANGAEA. https://doi.org/10.1594/PANGAEA.971116.
Lebreiro, Susana Martin, Antón López, Laura, Reguera, Isabel, Lozano, Rocio, 2025h. Element semiquantitative concentration of sediment core D11956TC/P [dataset]. PANGAEA. https://doi.org/10.1594/PANGAEA.971122.
Lebreiro, Susana Martin, Antón López, Laura, Reguera, Isabel, Lozano, Rocio, 2025i. Frequency of turbidites of sediment core MD03-2698 [dataset]. PANGAEA. https://doi.org/10.1594/PANGAEA.971120.
Lebreiro, Susana Martin, Antón López, Laura, Reguera, Isabel, Lozano, Rocio, 2025j. Magnetic susceptibility of sediment core D11956TC/P [dataset]. PANGAEA. https://doi.org/10.1594/PANGAEA.971121.
Lebreiro, Susana Martin, Antón López, Laura, Reguera, Isabel, Lozano, Rocio, 2025k. δ18O measurements of benthic foraminifera from sediment core MD13-3473 [dataset]. PANGAEA. https://doi.org/10.1594/PANGAEA.971114.
Lebreiro, S.M., Mccave, I., Weaver, P., 1997. Late Quaternary emplacement of turbidites on the horseshoe abyssal plain (iberian margin). J. Sediment. Res. 67, 856–870. https://doi.org/10.1306/D4268658-2B26-11D7-8648000102C1865D.
Lebreiro, S.M., Voelker, A.H.L., Vizcaino, A., Abrantes, F.G., Alt-Epping, U., Jung, S., et al., 2009. Sediment instability on the Portuguese continental margin under abrupt glacial climate changes (last 60kyr). Quat. Sci. Rev. 28 (27), 3211–3223. https://doi.org/10.1016/j.quascirev.2009.08.007.
Le Cann, B., Billant, A., Branellec, P., 2000. ARCANE - volume 1 : campagne ARCANE 98 - N/O Thalassa (23 juin - 22 juillet 1998) - rapport de données CTD-O2. Retrieved from. https://archimer.ifremer.fr/doc/00230/34132/.
Ledwell, J.R., Montgomery, E.T., Polzin, K.L., St Laurent, L.C., Schmitt, R.W., Toole, J. M., 2000. Evidence for enhanced mixing over rough topography in the abyssal ocean. Nature 403 (6766), 179–182. https://doi.org/10.1038/35003164.
Liang, X., Thurnherr, A.M., 2012. Eddy-modulated internal waves and mixing on a midocean ridge. J. Phys. Oceanogr. 42 (7), 1242–1248. https://doi.org/10.1175/JPO-D-11-0126.1.
Lister, C.R.B., 1976. Control of pelagic sediment distribution by internal waves of tidal period: possible interpretation of data from the southern East Pacific rise. Mar. Geol. 20 (4), 297–313. https://doi.org/10.1016/0025-3227(76)90109-2.
Löb, J., Köhler, J., Mertens, C., Walter, M., Li, Z., von Storch, J.-S., et al., 2020. Observations of the low-mode internal tide and its interaction with mesoscale flow south of the azores. J. Geophys. Res.: Oceans 125 (11), e2019JC015879. https://doi.org/10.1029/2019JC015879.
Lonsdale, P., Normark, W.R., Newman, W.A., 1972. Sedimentation and erosion on horizon guyot. GSA Bulletin 83 (2), 289–316. https://doi.org/10.1130/0016-7606(1972)83[289:SAEOHG]2.0.CO;2.
Lonsdale, P., 1976. Abyssal circulation of the southeastern Pacific and some geological implications. J. Geophys. Res. 81 (6), 1163–1176. https://doi.org/10.1029/JC081i006p01163.
MacCready, P., Rhines, P.B., 1993. Slippery bottom boundary layers on a slope. J. Phys. Oceanogr. 23 (1), 5–22. https://doi.org/10.1175/1520-0485(1993)023<0005:SBBLOA>2.0.CO;2.
MacKinnon, J.A., Zhao, Z., Whalen, C.B., Waterhouse, A.F., Trossman, D.S., Sun, O.M., et al., 2017. Climate process team on internal wave–driven ocean mixing. Bull. Am. Meteorol. Soc. 98 (11), 2429–2454. https://doi.org/10.1175/BAMS-D-16-0030.1.
Masson, D.G., Arzola, R.G., Wynn, R.B., Hunt, J., Weaver, P., 2011. Seismic triggering of landslides and turbidity currents offshore Portugal. G-cubed 12, 12011. https://doi.org/10.1029/2011GC003839.
Mérindol, M., St-Onge, G., Sultan, N., Lajeunesse, P., Garziglia, S., 2022. Earthquake-triggered submarine landslides in the st. Lawrence Estuary (québec, Canada) during the last two millennia and the record of the major 1663 CE M ≥7 event. Quat. Sci. Rev. 291, 107640. https://doi.org/10.1016/j.quascirev.2022.107640.
Miramontes, E., Penven, P., Fierens, R., Droz, L., Toucanne, S., Jorry, S.J., et al., 2019. The influence of bottom currents on the Zambezi valley morphology (mozambique channel, SW Indian Ocean): in situ current observations and hydrodynamic modelling. Mar. Geol. 410, 42–55. https://doi.org/10.1016/j.margeo.2019.01.002.
Nave, Silvia, Michel, E., 2013. MD 194/EUROFLEET - TORE Cruise. Marion Dufresne R/V. https://doi.org/10.17600/13200120.
Nave, Sílvia, Lebreiro, S., Michel, E., Kissel, C., Figueiredo, M.O., Guihou, A., et al., 2019. The Atlantic meridional overturning circulation as productivity regulator of the north Atlantic subtropical gyre. Quat. Res. 91 (1), 399–413. https://doi.org/10.1017/QUA.2018.88.
Nisbet, E., Piper, D.J.W., 1998. Giant submarine landslides. Nature 392 (6674), 329–330. https://doi.org/10.1038/32765.
Owen, M., Day, S., Maslin, M., 2007. Late Pleistocene submarine mass movements: occurrence and causes. Quat. Sci. Rev. 26, 958–978. https://doi.org/10.1016/j.quascirev.2006.12.011.
Peirce, C., Barton, P.J., 1991. Crustal structure of the madeira-tore rise, eastern North Atlantic—Results of a DOBS wide-angle and normal incidence seismic experiment in the josephine seamount region. Geophys. J. Int. 106 (2), 357–378. https://doi.org/10.1111/j.1365-246X.1991.tb03898.x.
Peliz, A., Dubert, J., Marchesiello, P., Teles-Machado, A., 2007. Surface circulation in the Gulf of Cadiz: model and mean flow structure. J. Geophys. Res.: Oceans 112 (C11). https://doi.org/10.1029/2007JC004159.
Peliz, A., Boutov, D., Cardoso, R.M., Delgado, J., Soares, P.M.M., 2013. The gulf of cadiz–alboran sea sub-basin: model setup, exchange and seasonal variability. Ocean Model. 61, 49–67. https://doi.org/10.1016/j.ocemod.2012.10.007.
Polzin, Kurt L., 2009. An abyssal recipe. Ocean Model. 30 (4), 298–309. https://doi.org/10.1016/j.ocemod.2009.07.006.
Polzin, K.L., Toole, J.M., Ledwell, J.R., Schmitt, R.W., 1997. Spatial variability of turbulent mixing in the abyssal Ocean. Science (New York, N.Y.) 276 (5309), 93–96. https://doi.org/10.1126/science.276.5309.93.
Posamentier, H.W., Vail, P., 1988. Eustatic controls on clastic deposition II – sequence and Systems Tract models. Sea-level changes: an integrated approach 42, 125–154. https://doi.org/10.2110/pec.88.01.0125.
Rahmstorf, S., 2003. Timing of abrupt climate change: a precise clock. Geophys. Res. Lett. 30 (10), 0.1029/2003GL017115.
Richardson, P.L., Bower, A.S., Zenk, W., 2000. A census of Meddies tracked by floats. Prog. Oceanogr. 45 (2), 209–250. https://doi.org/10.1016/S0079-6611(99)00053-1.
Rogerson, M., Colmenero-Hidalgo, E., Levine, R., Rohling, E.J., Voelker, A., Bigg, G., et al., 2010. Enhanced Mediterranean-Atlantic exchange during Atlantic freshening phases. G-cubed. https://doi.org/10.1029/2009GC002931.
Shanmugam, G., 2021. The turbidite-contourite-tidalite-baroclinite-hybridite problem: Orthodoxy vs. empirical evidence behind the “Bouma Sequence”. J. Palaeogeogr. 10, 1–32. https://doi.org/10.1186/s42501-021-00085-1.
Shanmugam, G., Moiola, R.J., 1982. Eustatic control of turbidites and winnowed turbidites. Geology 10 (5), 231–235. https://doi.org/10.1130/0091-7613(1982)10<231:ECOTAW>2.0.CO;2.
Shchepetkin, A.F., McWilliams, J.C., 2005a. The regional oceanic modeling system (ROMS): a split-explicit, free-surface, topography-following-coordinate oceanic model. Ocean Model. 9 (4), 347–404. https://doi.org/10.1016/j.ocemod.2004.08.002.
Shchepetkin, A., McWilliams, J.C., 2005b. CROCO (Coastal and Regional Ocean COmmunity model) version v2. https://zenodo.org/records/15064113.
Shu, Y., Wang, J., Xue, H., Huang, R.X., Chen, J., Wang, D., et al., 2022. Deep-current intraseasonal variability interpreted as topographic Rossby waves and deep eddies in the Xisha Islands of the South China Sea. J. Phys. Oceanogr. 52 (7), 1415–1430.
Siddall, M., Rohling, E.J., Thompson, W.G., Waelbroeck, C., 2008. Marine isotope stage 3 sea level fluctuations: data synthesis and new outlook. Rev. Geophys. 46 (4), 1–29. https://doi.org/10.1029/2007RG000226.
Siedler, G., Armi, L., Müller, T.J., 2005. Meddies and decadal changes at the Azores Front from 1980 to 2000. Deep Sea Res. Part II Top. Stud. Oceanogr. 52 (3), 583–604. https://doi.org/10.1016/j.dsr2.2004.12.010.
Sumner, E.J., Siti, M.I., McNeill, L.C., Talling, P.J., Henstock, T.J., Wynn, R.B., et al., 2013. Can turbidites be used to reconstruct a paleoearthquake record for the central Sumatran margin? Geology 41 (7), 763–766. https://doi.org/10.1130/G34298.1.
Toucanne, S., Zaragosi, S., Bourillet, J.F., Naughton, F., Cremer, M., Eynaud, F., et al., 2008. Activity of the turbidite levees of the Celtic–Armorican margin (Bay of Biscay) during the last 30,000 years: imprints of the last European deglaciation and Heinrich events. Mar. Geol. 247 (1–2), 84–103. https://doi.org/10.1016/j.margeo.2007.08.006.
Turnewitsch, R., Falahat, S., Nycander, J., Dale, A., Scott, R., Furnival, D., 2013. Deep-sea fluid and sediment dynamics—Influence of hill- to seamount-scale seafloor topography. Earth Sci. Rev. 127, 203–241. https://doi.org/10.1016/j.earscirev.2013.10.005.
Urlaub, M., Talling, P.J., Masson, D.G., 2013. Timing and frequency of large submarine landslides: implications for understanding triggers and future geohazard. Quat. Sci. Rev. 72, 63–82. https://doi.org/10.1016/j.quascirev.2013.04.020.
Vail, P.R., Jr, R.M.M., 1979. Global cycles of relative changes of sea level from seismic stratigraphy: resources, comparative structure, and eustatic changes in sea level. Geological and Geophysical Investigations of Continental Margins 109, 469–472. AAPG Special Volumes.
Vizcaíno, A., Gràcia, E., Pallàs, R., Garcia-Orellana, J., Escutia, C., Casas, D., et al., 2006. Sedimentology, physical properties and age of mass transport deposits associated with the Marques de Pombal Fault, Southwest Portuguese Margin. Nor. J. Geol. 86, 173–182. https://njg.geologi.no/vol-81-90/details/17/334-334.
Voelker, A., Lebreiro, S., Schonfeld, J., Cacho, I., Erlenkeuser, H., Abrantes, F., 2006. Mediterranean outflow strengthening during northern hemisphere coolings: a salt

source for the glacial Atlantic? Earth Planet Sci. Lett. 245 (1–2), 39–55. https://doi.org/10.1016/j.epsl.2006.03.014.
Voelker, A.H.L., Rodrigues, T., Billups, K., Oppo, D., McManus, J., Stein, R., et al., 2010. Variations in mid-latitude north Atlantic surface water properties during the mid-brunhes (MIS 9–14) and their implications for the thermohaline circulation. Clim. Past 6 (4), 531–552. https://doi.org/10.5194/cp-6-531-2010.
van Aken, H.M., 2000a. The hydrography of the mid-latitude northeast Atlantic Ocean: I: the deep water masses. Deep Sea Res. Oceanogr. Res. Pap. 47 (5), 757–788. https://doi.org/10.1016/S0967-0637(99)00092-8.
van Aken, H.M., 2000b. The hydrography of the mid-latitude northeast Atlantic Ocean: II: the intermediate water masses. Deep Sea Res. Oceanogr. Res. Pap. 47, 789–824, 0.1016/S0967-0637(99)00112-0.
van Haren, H., 2018. Abyssal plain hills and internal wave turbulence. Biogeosciences 15 (14), 4387–4403. https://doi.org/10.5194/bg-15-4387-2018.
van Haren, H., Cimatoribus, A., Gostiaux, L., 2015. Where large deep-ocean waves break. Geophys. Res. Lett. 42 (7), 2351–2357. https://doi.org/10.1002/2015GL063329.
Von Stackelberg, U., Von Rad, U., Zobel, B., 1979. Asymmetric sedimentation around great meteor seamount (north Atlantic). Mar. Geol. 33 (1), 117–132. https://doi.org/10.1016/0025-3227(79)90135-X.
Waelbroeck, C., Lougheed, B.C., Vazquez Riveiros, N., Missiaen, L., Pedro, J., Dokken, T., et al., 2019. Consistently dated Atlantic sediment cores over the last 40 thousand years. Sci. Data 6 (1), 165. https://doi.org/10.1038/s41597-019-0173-8.
Waelbroeck, C., Lougheed, B.C., Vazquez Riveiros, N., Missiaen, L., Pedro, J., Dokken, T., et al., 2022. Consistently dated Atlantic sediment cores over the last 40 thousand years. SEANOE. https://doi.org/10.17882/59554 [Data set].
Waelbroeck, C., Tjiputra, J., Guo, C., Nisancioglu, K.H., Jansen, E., Vázquez Riveiros, N., et al., 2023. Atlantic circulation changes across a stadial–interstadial transition. Clim. Past 19, 901–913. https://doi.org/10.5194/cp-19-901-2023.
Wang, J., Shu, Y., Wang, D., Xie, Q., Wang, Q., Chen, J., Zu, T., Liu, D., He, Y., 2021. Observed variability of bottom-trapped topographic rossby waves along the slope of the northern South China Sea. J. Geophys. Res.: Oceans 126 (12), e2021JC017746.
Weaver, P.P.E., Kuijpers, A., 1983. Climatic control of turbidite deposition on the madeira abyssal plain. Nature 306 (5941), 360–363. https://doi.org/10.1038/306360a0.
Weaver, P.P.E., Rothwell, R.G., Ebbing, J., Gunn, D., Hunter, P.M., 1992. Correlation, frequency of emplacement and source directions of megaturbidites on the madeira abyssal plain. Mar. Geol. 109 (1), 1–20. https://doi.org/10.1016/0025-3227(92)90218-7.
White, M., Mohn, C., 2002. Seamounts: a review of physical processes and their influence on the seamount ecosystem. In: Oasis Rep Contract, vol. 38. National University Ireland.
Wilmes, S.-B., Green, J.A.M., 2014. The evolution of tides and tidal dissipation over the past 21,000 years. J. Geophys. Res.: Oceans 119 (7), 4083–4100. https://doi.org/10.1002/2013JC009605.
Wilmes, S.-B., Schmittner, A., Green, J.A.M., 2019. Glacial ice sheet extent effects on modeled tidal mixing and the global overturning circulation. Paleoceanogr. Paleoclimatol. 34 (8), 1437–1454. https://doi.org/10.1029/2019PA003644.
Wu, L., Wilson, D.J., Wang, R., Yin, X., Chen, Z., Xiao, W., et al., 2020. Evaluating Zr/Rb ratio from XRF scanning as an indicator of grain-size variations of glaciomarine sediments in the Southern Ocean. G-cubed 21 (11), e2020GC009350. https://doi.org/10.1029/2020GC009350.
Xie, X., Wang, Y., Liu, Z., Liu, X., Chen, D., Zhang, D., et al., 2023. Observation of near-inertial waves in the bottom boundary layer of an abyssal seamount. J. Phys. Oceanogr. 53 (2), 635–645.
Yang, Z., Jing, Z., Zhai, X., Vic, C., Sun, H., de Lavergne, C., et al., 2024. Enhanced generation of internal tides under global warming. Nat. Commun. 15 (1), 7657. https://doi.org/10.1038/s41467-024-52073-3.